Chapter 6

Reflection and transmission of plane waves

If a pencil of WHITE *light polarised by reflexion is incident at the polarising angle upon any transparent surface, so that the plane of the second reflexion is at right angles to the plane of its primitive polarisation, a portion of the pencil consisting of the mean refrangible rays will lose its reflexibility, and will entirely penetrate the second surface, while another portion of the beam, composed of the blue and red rays, will not lose its reflexibility, but will suffer reflexion and refraction like ordinary light.*

David Brewster (Brewster, 1815)

The reflection and transmission problem at an interface between anisotropic anelastic media is a complex phenomenon. A general approach has, in this case, the disadvantage of limiting the depth to which we can study the problem analytically and precludes us from gaining further physical insight into the nature of the problem. In this chapter, the main physical results are illustrated by considering relatively simple cases, that is, propagation of SH waves in the plane of symmetry of monoclinic media, and propagation of qP-qSV waves in a plane containing the axes of symmetry of transversely isotropic media. In both cases, the refracting boundary is plane and perpendicular to the symmetry planes.

The problem of reflection and transmission at an interface between two anelastic transversely isotropic media whose symmetry axes are perpendicular to the interface has a practical application in the exploration for hydrocarbon reservoirs using seismic waves. The interface may separate two finely layered formations whose contact plane is parallel to the stratification. Anelastic rheology models the different attenuation mechanisms resulting from the presence of cracks and fluid saturation.

We have seen in Chapters 3 and 4 that the most relevant difference from the elastic case is the presence of inhomogeneous waves which have a body-wave character, in contrast to the inhomogeneous waves of the elastic type, which propagate along interfaces. For viscoelastic inhomogeneous waves, the angle between the propagation and attenuation vectors is strictly less than 90°, unlike inhomogeneous waves in elastic media. In addition, depending on the inhomogeneity of the wave, its behavior (e.g., phase velocity, attenuation, particle motion) may also differ substantially. Moreover, as we have seen in Chapter 1, in the anisotropic case, the energy-flow direction, in general, does not coincide with the propagation (wavevector) direction, and critical angles occur when the ray (energy-

flow) direction is parallel to the interface. The theoretical developments presented in this chapter follow from Carcione (1997a,b).

6.1 Reflection and transmission of SH waves

The cross-plane shear problem is one of relative mathematical simplicity and includes the essential physics common to more complicated cases, where multiple and coupled deformations occur (Horgan, 1995). In this sense, analysis of the reflection and transmission of cross-plane shear waves serves as a pilot problem for investigating the influence of anisotropy and/or anelasticity on solution behavior. As is well known, propagation in the plane of mirror symmetry of a monoclinic medium is the most general situation for which cross-plane strain motion exists in all directions – the corresponding waves are also termed type-II S and SH in the geophysical literature (Borcherdt, 1977; Helbig, 1994).

Besides the work of Hayes and Rivlin (1974), who considered a low-loss approximation, the study of wave propagation in anisotropic viscoelastic media is a relatively recent topic. In the following discussion, we consider two monoclinic media with a common mirror plane of symmetry in contact along a plane perpendicular to the symmetry plane. The incidence and refraction planes are assumed to be coincident with this plane of symmetry. Then, an incident cross-plane shear wave will generate reflected and transmitted shear waves without conversion to the coupled quasi-compressional and quasi-shear modes.

The physics of the problem may differ depending on the values of the elasticity constants and the anisotropic dissipation of the upper and lower media. For this reason, we follow a general treatment and, simultaneously, consider a numerical example including the essential physical aspects. In this way, the analysis provides further insight into the nature of the reflection and transmission problem.

6.1.1 Symmetry plane of a homogeneous monoclinic medium

Assume a homogeneous and viscoelastic monoclinic medium with the vertical (x,z)-plane as its single symmetry plane. Then, cross-plane shear waves with particle velocity $\mathbf{v} = v(x,z)\hat{\mathbf{e}}_2$ propagate such that

$$v = \mathrm{i}\omega u_0 \exp[\mathrm{i}\omega(t - s_1 x - s_3 z)], \tag{6.1}$$

where s_1 and s_3 are the components of the complex-slowness vector, ω is the angular frequency satisfying $\omega \geq 0$, and u_0 is a complex quantity. The slowness and attenuation vectors are given by

$$\mathbf{s}_R = (\mathrm{Re}(s_1), \mathrm{Re}(s_3)) \tag{6.2}$$

and

$$\boldsymbol{\alpha} = -\omega(\mathrm{Im}(s_1), \mathrm{Im}(s_3)), \tag{6.3}$$

respectively, such that the complex-slowness vector is $\mathbf{s} = \mathbf{s}_R - \mathrm{i}(\boldsymbol{\alpha}/\omega)$.

The cross-plane assumption implies that σ_{12} and σ_{32} are the only non-zero components of stress that satisfy the stress-strain relations

$$\mathrm{i}\omega\sigma_{12} = p_{46}\partial_3 v + p_{66}\partial_1 v, \quad \text{and} \quad \mathrm{i}\omega\sigma_{32} = p_{44}\partial_3 v + p_{46}\partial_1 v, \tag{6.4}$$

where p_{IJ} are the complex stiffnesses (see Sections 4.1 and 4.6). These complex stiffnesses equal the real high-frequency limit elasticity constants c_{IJ} in the elastic case.

The complex-slowness relation has the following simple form:

$$F(s_1, s_3) \equiv p_{44}s_3^2 + p_{66}s_1^2 + 2p_{46}s_1s_3 - \rho = 0. \tag{6.5}$$

(See the elastic version in equation (1.261).)

Let us assume that the positive z-axis points downwards. In order to distinguish between down and up propagating waves, the slowness relation is solved for s_3, given the horizontal slowness s_1. It yields

$$s_{3\pm} = \frac{1}{p_{44}}\left(-p_{46}s_1 \pm \mathrm{pv}\sqrt{\rho p_{44} - p^2 s_1^2}\right), \tag{6.6}$$

where

$$p^2 = p_{44}p_{66} - p_{46}^2 \tag{6.7}$$

and $\mathrm{pv}\sqrt{w}$ denotes the principal value of the square root of the complex number w. In principle, the + sign corresponds to downward or $+z$ propagating waves, while the − sign corresponds to upward or $-z$ propagating waves.

We recall that, as shown in Section 1.4.2, the group velocity equals the energy velocity only when there is no attenuation. Therefore, analysis of the physics requires explicit calculation of the energy velocity, since the concept of group velocity loses its physical meaning in anelastic media (see Section 4.4.5). The mean energy flux or time-averaged Umov-Poynting vector $\langle \mathbf{p} \rangle$ is the real part of the corresponding complex vector

$$\mathbf{p} = -\frac{1}{2}(\sigma_{12}\hat{\mathbf{e}}_1 + \sigma_{32}\hat{\mathbf{e}}_3)v^* \tag{6.8}$$

(equation (4.111)). Substituting the plane wave (6.1) and the stress-strain relations (6.4) into equation (6.8), we obtain

$$\mathbf{p} = \frac{1}{2}\omega^2|u_0|^2 \exp\{2\omega[\mathrm{Im}(s_1)x + \mathrm{Im}(s_3)z]\}(X\hat{\mathbf{e}}_1 + Z\hat{\mathbf{e}}_3), \tag{6.9}$$

where

$$X = p_{66}s_1 + p_{46}s_3, \quad \text{and} \quad Z = p_{46}s_1 + p_{44}s_3. \tag{6.10}$$

For time harmonic fields, the time-averaged strain- and dissipated-energy densities, $\langle V \rangle$ and $\langle D \rangle$, can be obtained from a complex strain-energy density Φ. This can be deduced from equations (4.53), (4.54), (4.85) and (6.4). Hence, we have

$$\Phi = \frac{1}{2}\,\mathbf{e}^\top \cdot \mathbf{P} \cdot \mathbf{e}^*, \tag{6.11}$$

which for SH waves propagating in a monoclinic medium is given by

$$\Phi = \frac{1}{2}\left\{p_{44}\left|\frac{\partial_3 v}{\mathrm{i}\omega}\right|^2 + p_{66}\left|\frac{\partial_1 v}{\mathrm{i}\omega}\right|^2 + 2p_{46}\mathrm{Re}\left[\frac{\partial_3 v}{\mathrm{i}\omega}\left(\frac{\partial_1 v}{\mathrm{i}\omega}\right)^*\right]\right\}. \tag{6.12}$$

(The demonstration is left to the reader.) Then,

$$\langle V \rangle = \frac{1}{2}\mathrm{Re}(\Phi), \qquad \langle D \rangle = \mathrm{Im}(\Phi). \tag{6.13}$$

Substituting the plane wave (6.1) into (6.12), we find that the energy densities become

$$\langle V \rangle = \frac{1}{4}\omega^2 |u_0|^2 \exp\{2\omega[\mathrm{Im}(s_1)x + \mathrm{Im}(s_3)z]\}\mathrm{Re}(\varrho) \tag{6.14}$$

and

$$\langle D \rangle = \frac{1}{2}\omega^2 |u_0|^2 \exp\{2\omega[\mathrm{Im}(s_1)x + \mathrm{Im}(s_3)z]\}\mathrm{Im}(\varrho), \tag{6.15}$$

where

$$\varrho = p_{44}|s_3|^2 + p_{66}|s_1|^2 + 2p_{46}\mathrm{Re}(s_1^* s_3). \tag{6.16}$$

From equation (4.52), we obtain the time-averaged kinetic-energy density, namely,

$$\langle T \rangle = \frac{1}{4}\rho|v^2| = \frac{1}{4}\rho\omega^2|u_0|^2 \exp\{2\omega[\mathrm{Im}(s_1)x + \mathrm{Im}(s_3)z]\}. \tag{6.17}$$

6.1.2 Complex stiffnesses of the incidence and transmission media

A realistic viscoelastic model is the Zener model (see Section 2.4.3). It satisfies causality and gives relaxation and creep functions in agreement with experimental results (e.g., aluminum (Zener, 1948) and shale (Johnston, 1987)).

We assign different Zener elements to p_{44} and p_{66} in order to define the attenuation (or quality factor) along the horizontal and vertical directions (x- and z-axes), respectively. Hence, the stiffnesses are

$$p_{44} = c_{44}M_1, \quad p_{66} = c_{66}M_2, \quad p_{46} = c_{46}, \tag{6.18}$$

where

$$M_\nu = \frac{\tau_{\sigma\nu}}{\tau_{\epsilon\nu}}\left(\frac{1 + \mathrm{i}\omega\tau_{\epsilon\nu}}{1 + \mathrm{i}\omega\tau_{\sigma\nu}}\right), \quad \nu = 1, 2 \tag{6.19}$$

are the complex moduli (see Section 2.4.3). The relaxation times are given by

$$\tau_{\epsilon\nu} = \frac{\tau_0}{Q_{0\nu}}\left(\sqrt{Q_{0\nu}^2 + 1} + 1\right), \quad \tau_{\sigma\nu} = \frac{\tau_0}{Q_{0\nu}}\left(\sqrt{Q_{0\nu}^2 + 1} - 1\right), \tag{6.20}$$

where τ_0 is a characteristic relaxation time and $Q_{0\nu}$ is a characteristic quality factor. An alternative form of the complex modulus is given by equation (4.6). It can be shown from equations (2.201), (4.92) and (4.106), that the quality factors for homogeneous waves along the axes are

$$Q_\nu = Q_{0\nu}\left(\frac{1 + \omega^2\tau_0^2}{2\omega\tau_0}\right). \tag{6.21}$$

Then, $1/\tau_0$ is the angular frequency for which the quality factor has the minimum value $Q_{0\nu}$. The choice $\tau_0 = \sqrt{\tau_{\epsilon 1}\tau_{\sigma 1}} = \sqrt{\tau_{\epsilon 2}\tau_{\sigma 2}}$ implies that the maximum dissipation for both mechanisms occurs at the same frequency. As $\omega \to \infty$, $M_\nu \to 1$ and the complex stiffnesses p_{IJ} approach the unrelaxed elasticity constants c_{IJ}.

In the reflection-transmission problem, the upper medium is defined by the properties c_{IJ}, $Q_{0\nu}$ and τ_0, and the lower medium is defined by the corresponding primed properties c'_{IJ}, $Q'_{0\nu}$ and τ'_0. The numerical example assumes

$$\begin{array}{llll} c_{44} = 9.68 \text{ GPa}, & Q_{01} = 10, \\ c_{66} = 12.5 \text{ GPa}, & Q_{02} = 20, \\ c'_{44} = 19.6 \text{ GPa}, & Q'_{01} = 20, \\ c'_{66} = 25.6 \text{ GPa}, & Q'_{02} = 30. \end{array} \tag{6.22}$$

Moreover,

$$c_{46} = -\frac{1}{2}\sqrt{c_{44}c_{66}}, \qquad c'_{46} = \frac{1}{2}\sqrt{c'_{44}c'_{66}}, \tag{6.23}$$

and

$$\rho = 2 \text{ gr/cm}^3, \qquad \rho' = 2.5 \text{ gr/cm}^3. \tag{6.24}$$

The characteristic relaxation time is taken as $\tau_0 = \tau'_0 = (2\pi f_0)^{-1}$, i.e., the maximum attenuation occurs at a frequency f_0. The above parameters give horizontal and vertical (elastic or unrelaxed) phase velocities of 2500 m/s and 2200 m/s, respectively, for the upper medium, and 3200 m/s and 2800 m/s, respectively, for the lower medium.

Several subcases treated in the analysis make use of the following limiting situations:

$$\begin{array}{ll} \text{elastic :} & Q_{0\nu} = Q'_{0\nu} = \infty \ (\tau_{\epsilon\nu} = \tau_{\sigma\nu},\ \tau'_{\epsilon\nu} = \tau'_{\sigma\nu}) \ \text{ or } \ M_\nu = M'_\nu = 1, \\ \text{isotropic :} & p_{44} = p_{66} = \mu,\ p'_{44} = p'_{66} = \mu',\ p_{46} = p'_{46} = 0, \\ \text{transversely isotropic :} & p_{46} = p'_{46} = 0. \end{array} \tag{6.25}$$

Note, however, that the condition $p_{46} = p'_{46} = 0$ does not necessarily mean that the media are transversely isotropic (see Section 1.2.1).

The analysis of the problem is carried out at the frequency f_0 and, therefore, its value is immaterial, because $\omega\tau_0 = 1$ Moreover, at a fixed frequency, the analysis does not depend on the viscoelastic model.

6.1.3 Reflection and transmission coefficients

Let us assume that the incident, reflected and transmitted waves are identified by the superscripts I, R and T. The solution to the problem parallels those of the anisotropic elastic case (Section 1.9.1) and isotropic viscoelastic case (Section 3.8).

The particle velocity of the incident wave can be written as

$$v^I = \mathrm{i}\omega \exp[\mathrm{i}\omega(t - s_1 x - s_3^I z)], \tag{6.26}$$

where, for simplicity, the superscript I in the horizontal slowness has been omitted here and in all the subsequent analysis.

Inhomogeneous viscoelastic plane waves have the property that equiphase planes – planes normal to the slowness vector – do not coincide with equiamplitude planes – planes normal to the attenuation vector. When the directions of propagation and attenuation coincide, the wave is called homogeneous. For a homogeneous wave (see Section 4.2),

$$s_1 = \sin\theta^I / v_c(\theta^I), \qquad s_3^I = \cos\theta^I / v_c(\theta^I), \tag{6.27}$$

where θ^I is the incidence propagation – or attenuation – angle (see Figure 6.1), and

$$v_c(\theta) = \sqrt{(p_{44}\cos^2\theta + p_{66}\sin^2\theta + p_{46}\sin 2\theta)/\rho} \tag{6.28}$$

is the complex velocity, according to the dispersion relation (6.5) and equations (4.28) and (4.33).

As in the isotropic viscoelastic case (Section 3.8), the boundary conditions – continuity of v and σ_{32} – give the reflection and transmission coefficients. Snell's law, i.e., the continuity of the horizontal complex slowness,

$$s_1^R = s_1^T = s_1, \tag{6.29}$$

(see Section 3.5) is a necessary condition for the existence of the boundary conditions.

Denoting the reflection and transmission coefficients by R_{SS} and T_{SS}, we express the particle velocities of the reflected and transmitted waves as

$$v^R = \mathrm{i}\omega R_{\mathrm{SS}} \exp[\mathrm{i}\omega(t - s_1 x - s_3^R z)] \tag{6.30}$$

and

$$v^T = \mathrm{i}\omega T_{\mathrm{SS}} \exp[\mathrm{i}\omega(t - s_1 x - s_3^T z)], \tag{6.31}$$

respectively.

Then, continuity of v and σ_{32} at $z = 0$ gives

$$T_{\mathrm{SS}} = 1 + R_{\mathrm{SS}} \tag{6.32}$$

and

$$Z_I + R_{\mathrm{SS}} Z_T = T_{\mathrm{SS}} Z_T, \tag{6.33}$$

which have the following solution:

$$R_{\mathrm{SS}} = \frac{Z^I - Z^T}{Z^T - Z^R}, \qquad T_{\mathrm{SS}} = \frac{Z^I - Z^R}{Z^T - Z^R}. \tag{6.34}$$

Since both the incident and reflected waves satisfy the slowness relation (6.5), the vertical slowness s_3^R can be obtained by subtracting $F(s_1, s_3^I)$ from $F(s_1, s_3^R)$ and assuming $s_3^R \neq s_3^I$. This yields

$$s_3^R = -\left(s_3^I + \frac{2p_{46}}{p_{44}} s_1\right). \tag{6.35}$$

Then, using equation (6.10), we obtain

$$Z^R = -Z^I, \tag{6.36}$$

and the reflection and transmission coefficients (6.34) become

$$R_{\mathrm{SS}} = \frac{Z^I - Z^T}{Z^I + Z^T}, \qquad T_{\mathrm{SS}} = \frac{2Z^I}{Z^I + Z^T}, \tag{6.37}$$

where

$$Z^I = p_{46} s_1 + p_{44} s_3^I \quad \text{and} \quad Z^T = p'_{46} s_1 + p'_{44} s_3^T. \tag{6.38}$$

The slowness relation (6.5) of the transmission medium gives s_3^T in terms of s_1:

$$s_3^T = \frac{1}{p'_{44}}\left(-p'_{46}s_1 + \mathrm{pv}\sqrt{\rho' p'_{44} - p'^2 s_1^2}\right), \tag{6.39}$$

with

$$p'^2 = p'_{44}p'_{66} - {p'_{46}}^2. \tag{6.40}$$

Alternatively, from equation (6.10),

$$s_3^T = \frac{1}{p'_{44}}\left(Z^T - p'_{46}s_1\right). \tag{6.41}$$

Figure 6.1 represents the incident (I), reflected (R) and transmitted (T) waves at a boundary between two linear viscoelastic and monoclinic media. The angles θ, δ and ψ denote the propagation, attenuation and Umov-Poynting vector (energy) directions. Note that the propagation and energy directions do not necessarily coincide. Moreover, $|\theta - \delta|$ may exceed 90^o in anisotropic viscoelastic media, while $|\theta - \delta|$ is strictly less than 90^o in isotropic media (see equation (3.36)).

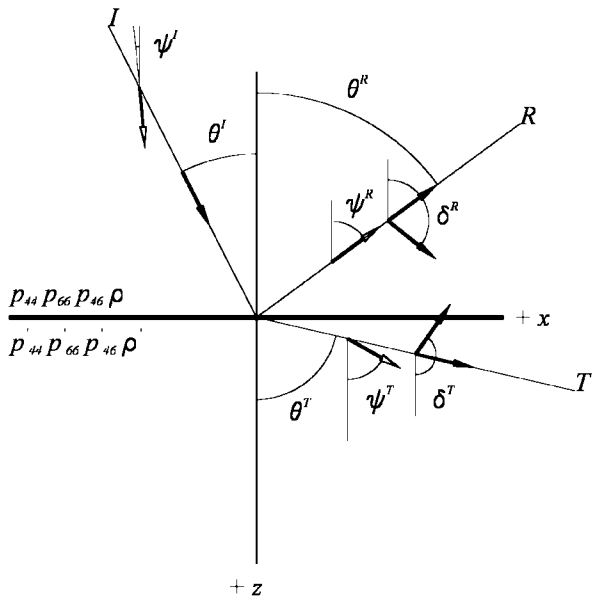

Figure 6.1: Incident (I), reflected (R) and transmitted (T) waves at a boundary between two linear viscoelastic and monoclinic media. The angles θ, δ and ψ denote the propagation, attenuation and Umov-Poynting vector (energy) directions. The reflection angle is negative as shown.

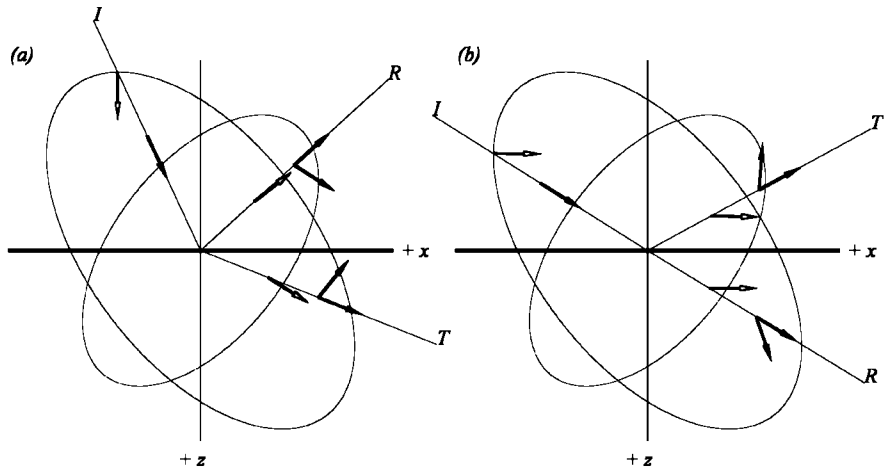

Figure 6.2: Limiting rays for the fan of incidence angles. (a) $\theta^I = 24.76^o$ and (b) $\theta^I = 58.15^o$ (23.75^o and 60.39^o, respectively, in the elastic case). They are determined by the condition that the energy propagation direction is downwards ($+z$) and to the right ($+x$), i.e., $0 \leq \psi^I \leq 90^o$. The larger curve is the slowness for homogeneous waves in the incidence medium and the other curve is the slowness for homogeneous waves in the transmission medium.

6.1.4 Propagation, attenuation and energy directions

The fan of incident rays is determined by the condition that the energy propagation direction is downwards ($+z$) and to the right ($+x$). The limiting rays for the numerical example are represented in Figures 6.2a ($\theta^I = 24.76^o$) and 6.2b ($\theta^I = 58.15^o$) (23.75^o and 60.39^o, respectively, in the elastic case). The larger curve is the slowness for homogeneous waves in the incidence medium, and the other curve is the slowness for homogeneous waves in the transmission medium. As we have seen in Section 4.4.4, the energy direction is not perpendicular to the corresponding slowness curve for all frequencies. The perpendicularity property is only verified in the low- and high-frequency limits.

Given the components of the complex-slowness vector, the propagation and attenuation angles θ and δ for all the waves are

$$\tan\theta = \frac{\mathrm{Re}(s_1)}{\mathrm{Re}(s_3)} \tag{6.42}$$

and

$$\tan\delta = \frac{\mathrm{Im}(s_1)}{\mathrm{Im}(s_3)}. \tag{6.43}$$

These equations can be easily verified for the incident wave (6.26), for which $\delta^I = \theta^I$, by virtue of equation (6.27).

Moreover, from equations (6.30) and (6.35), the reflection propagation and attenuation angles are

$$\tan\theta^R = -\frac{\mathrm{Re}(s_1)}{\mathrm{Re}(s_3^I + 2p_{46}p_{44}^{-1}s_1)} \tag{6.44}$$

and

$$\tan\delta^R = -\frac{\mathrm{Im}(s_1)}{\mathrm{Im}(s_3^I + 2p_{46}p_{44}^{-1}s_1)}, \tag{6.45}$$

respectively. Unlike the isotropic case, the reflected wave is, in general, inhomogeneous.

Theorem 1: If the incident wave is homogeneous and not normally incident, the reflected wave is homogeneous if and only if $\mathrm{Im}(p_{46}/p_{44}) = 0$.

Proof: Assume that the reflected wave is homogeneous. Then, from equations (6.44) and (6.45), $\tan\theta^R = \tan\delta^R$ implies that $\mathrm{Im}[s_1^*(s_3^I + 2p_{46}p_{44}^{-1}s_1)] = 0$. Assuming $\theta^I \neq 0$ and using equation (6.27), we obtain $\mathrm{Im}(p_{46}/p_{44}) = 0$. The same reasoning shows that this condition implies a homogeneous reflected wave. ♣

A corollary of Theorem 1 is

Corollary 1.1: If the upper medium has $p_{46} = 0$, the reflected wave is homogeneous. This follows immediately from Theorem 1.

In the elastic case, all the quantities in equation (6.44) are real, and the incidence and reflection angles are related by

$$\cot\theta^R = -\left(\cot\theta^I + 2\frac{c_{46}}{c_{44}}\right). \tag{6.46}$$

From equation (6.31), the transmission propagation and attenuation angles are

$$\tan\theta^T = \frac{\mathrm{Re}(s_1)}{\mathrm{Re}(s_3^T)} \tag{6.47}$$

and

$$\tan\delta^T = \frac{\mathrm{Im}(s_1)}{\mathrm{Im}(s_3^T)}, \tag{6.48}$$

respectively. In general, the transmitted wave is inhomogeneous.

Theorem 2: If the transmission medium is elastic and the incidence is non-normal, the attenuation and Umov-Poynting vectors of the transmitted wave are perpendicular, i.e., $|\psi^T - \delta^T| = 90^o$.

Proof: In the first place, $\boldsymbol{\alpha}^T$ must be different from zero at non-normal incidence, because the incident wave is homogeneous, and, therefore, Snell's law requires a non-zero component of the attenuation vector. The time-averaged dissipated-energy density for cross-plane inhomogeneous waves in the plane of symmetry of a monoclinic medium is given by equation (6.15) (see also Krebes and Le, 1994; and Carcione and Cavallini, 1995a). For the transmitted wave, it is

$$\langle D^T\rangle = \frac{1}{2}\omega^2|T_{\mathrm{SS}}|^2\exp\{2\omega[\mathrm{Im}(s_1)x + \mathrm{Im}(s_3^T)z]\}\mathrm{Im}(\varrho^T), \tag{6.49}$$

where

$$\varrho^T = p'_{44}|s_3^T|^2 + p'_{66}|s_1|^2 + 2p'_{46}\mathrm{Re}(s_1^* s_3^T). \tag{6.50}$$

Since the medium is elastic ($p'_{IJ} \rightarrow c'_{IJ}$), ϱ^T is real and $\langle D^T\rangle = 0$. On the other hand, equations (4.83) and (4.85) imply that an inhomogeneous wave satisfies

$$\langle D^T\rangle = \frac{2}{\omega}\boldsymbol{\alpha}^T \cdot \langle \mathbf{p}^T\rangle. \tag{6.51}$$

Since the energy loss is zero, it is clear from equation (6.51) that $\boldsymbol{\alpha}^T$ is perpendicular to the average Umov-Poynting vector $\langle \mathbf{p}^T \rangle$. ♣

The existence of an inhomogeneous plane wave propagating away from the interface in elastic media, is not intuitively obvious, since it is not the usual interface wave with its attenuation vector perpendicular to the boundary. Such body waves appear, for instance, in the expansion of a spherical wave (Brekhovskikh, 1960, p. 240).

Corollary 2.1: Theorem 2 implies that, in general, the attenuation direction of the transmitted wave is not perpendicular to the propagation direction. That is, $\boldsymbol{\alpha}^T \cdot \mathbf{s}_R^T \neq 0$, or

$$\mathrm{Re}(s_1)\mathrm{Im}(s_1) + \mathrm{Re}(s_3^T)\mathrm{Im}(s_3^T) \neq 0, \tag{6.52}$$

which implies $\mathrm{Im}(s_1^2 + s_3^{T2}) = 0$. The orthogonality property only applies in the isotropic case (Romeo, 1994). Assume, for simplicity, transverse isotropy. Using (6.52) and the slowness relation (6.5), we obtain

$$\mathrm{Im}(s_1^2)(c'_{66} - c'_{44}) = 0, \tag{6.53}$$

which gives $c'_{66} = c'_{44}$, that is, the isotropic case.

Proposition 1: If the incidence medium is elastic, the attenuation of the transmitted wave is perpendicular to the interface.

This result follows immediately from equation (6.48), since s_1 real (see equation (6.27)) implies $\delta^T = 0$. ♣

The expressions for the time-averaged Umov-Poynting vectors of the reflected and transmitted waves, are obtained from equation (6.9), with $u_0 = R_{\mathrm{SS}}$ and $u_0 = T_{\mathrm{SS}}$, respectively. Then, the angles of the reflection and transmission energy vectors are obtained from

$$\tan\psi^I = \frac{\mathrm{Re}(X^I)}{\mathrm{Re}(Z^I)}, \tag{6.54}$$

$$\tan\psi^R = \frac{\mathrm{Re}(X^R)}{\mathrm{Re}(Z^R)} \tag{6.55}$$

and

$$\tan\psi^T = \frac{\mathrm{Re}(X^T)}{\mathrm{Re}(Z^T)}, \tag{6.56}$$

respectively. From equations (6.10) and (6.35) $Z^R = -Z^I$ and $X^R = X^I - 2p_{46}p_{44}^{-1}Z^I$; therefore,

$$\tan\psi^R = \frac{2\mathrm{Re}(p_{46}p_{44}^{-1}Z^I)}{\mathrm{Re}(Z^I)} - \tan\psi^I. \tag{6.57}$$

In the elastic case p_{46} and p_{44} are real and

$$\tan\psi^R = 2\frac{c_{46}}{c_{44}} - \tan\psi^I. \tag{6.58}$$

In the evaluation of each angle, particular attention should be given to the choice of the branch of the arctangent.

Figure 6.3 represents the propagation, attenuation and energy angles for the fan of incident rays. Note that the energy angle of the incident wave satisfies $0^o \leq \psi^I \leq 90^o$ and that the inhomogeneity angles of the reflected and transmitted waves – $|\theta^R - \delta^R|$ and

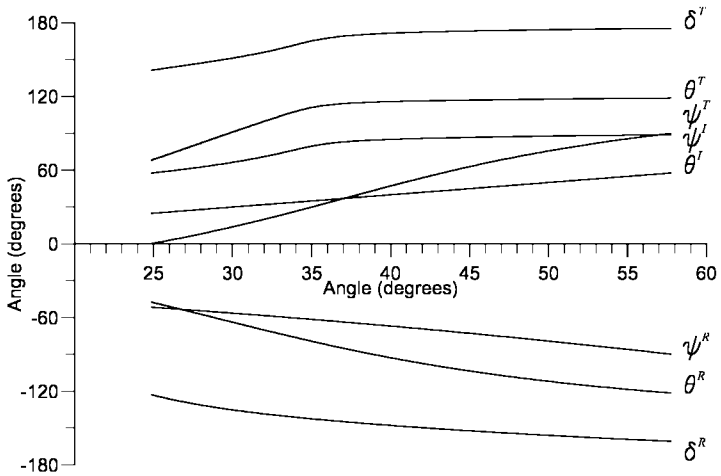

Figure 6.3: Propagation, attenuation and energy angles for the incident, reflected and transmitted waves versus the incidence angle θ^I.

$|\theta^T - \delta^T|$, respectively – never exceed 90^o. However, consider a transmission medium with stronger dissipation, for instance, $Q'_{01} = 2$ and $Q'_{02} = 3$. In this case, $|\theta^T - \delta^T| > 90^o$ for $\theta^I \geq 50.46^o$, meaning that the amplitude of the transmitted wave grows in the direction of phase propagation. A physical interpretation of this phenomenon is given by Krebes and Le (1994) who show that the amplitude of an inhomogeneous wave decays in the direction of energy propagation, i.e., in our case, $|\psi^T - \delta^T|$ is always less than 90^o. Indeed, since the energy loss is always positive, equation (6.51) implies that the magnitude of the angle between $\boldsymbol{\alpha}^T$ and $\langle \mathbf{p}^T \rangle$ is always strictly less than 90^o.

Proposition 2: There is an incidence angle θ_0^I such that the incidence and reflection propagation directions coincide, i.e., $\theta_0^I - \theta^R = 180^o$.

The angle can be found by equating (6.42) (for the incident wave) with (6.44) and using equation (6.10). This yields

$$\mathrm{Re}(Z^I/p_{44}) = 0, \tag{6.59}$$

whose solution is $\theta_0^I = 58.15^o$, which corresponds to Figure 6.2b. In the elastic case, we obtain

$$\theta_0^I = -\arctan(c_{44}/c_{46}), \tag{6.60}$$

whose solution is $\theta_0^I = 60.39^o$. The angle is 90^o in the isotropic case. ♣

Proposition 3: There is an incidence angle θ_1^I such that the reflection and transmission propagation directions coincide, i.e., $\theta^T - \theta^R = 180^o$.

The angle is obtained from equations (6.44) and (6.47) and the solution is $\theta_1^I = 33.40^o$, with $\theta^R = -74.46^o$. There is an explicit expression in the elastic case that can be obtained from equations (6.27), (6.28), (6.39), (6.44) and (6.47). It is

$$\tan\theta_1^I = (-b - \sqrt{b^2 - 4ac})/(2a), \tag{6.61}$$

where

$$\begin{aligned} a &= \rho' c_{66} - \rho c'_{66} + 4\rho c_{46}(c'_{46}c_{44} - c_{46}c'_{44})/c_{44}^2, \\ b &= 2(\rho' c_{46} + \rho c'_{46} - 2\rho c_{46}c'_{44}/c_{44}), \\ c &= \rho' c_{44} - \rho c'_{44}. \end{aligned} \tag{6.62}$$

The solutions are $\theta_1^I = 34.96^o$ and $\theta^R = -73.63^o$. In the isotropic case, $a = c$, $b = 0$ and there is no solution. ♣

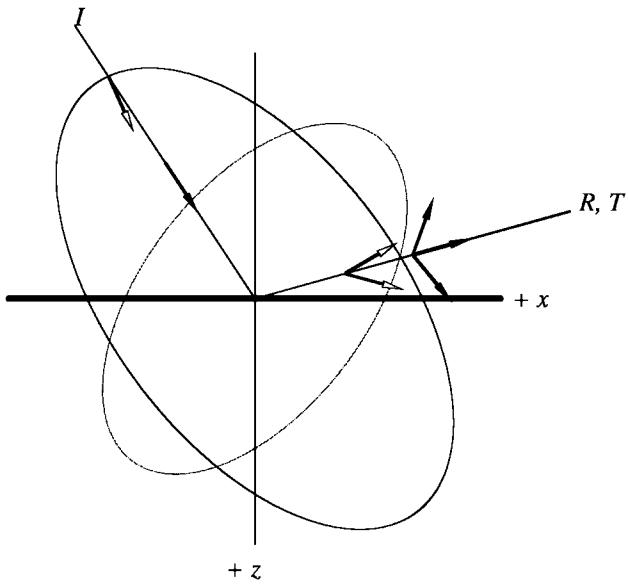

Figure 6.4: At the incidence angle $\theta_1^I = 33.40^o$, the reflection and transmission propagation directions coincide. However, note that the Umov-Poynting vector of the transmitted wave (empty arrow) points downward.

This situation is shown in Figure 6.4, where the Umov-Poynting and attenuation vectors of the reflected wave point upward and downward, respectively, while the Umov-Poynting and attenuation vectors of the transmitted wave point downward and upward, respectively. Thus, there is no contradiction since the energy of the transmitted wave is actually pointing to the lower medium.

Proposition 4: There is an incidence angle θ_2^I such that the propagation direction of the incident wave coincides with the corresponding Umov-Poynting vector direction, i.e., $\theta^I = \psi^I = \theta_2^I$. This angle is associated with the symmetry axis of the incidence medium, which is a pure mode direction where the waves behave as in isotropic media.

From equations (6.42) and (6.54), we note that this proposition is verified when

$$\frac{\mathrm{Re}(s_1)}{\mathrm{Re}(s_3^I)} = \frac{\mathrm{Re}(X^I)}{\mathrm{Re}(Z^I)}. \tag{6.63}$$

Using equations (6.10) and (6.27), and after some algebra, we obtain an approximation for $Q_{0\nu} \gg 1$ ($\mathrm{Im}(v_c) \ll \mathrm{Re}(v_c)$):

$$\tan\theta_2^I = \left\{ \mathrm{Re}(p_{66} - p_{44}) - \sqrt{[\mathrm{Re}(p_{66} - p_{44})]^2 + 4[\mathrm{Re}(p_{46})]^2} \right\} / [2\mathrm{Re}(p_{46})]. \tag{6.64}$$

The solution is $\theta_2^I = 36.99^o$ (the exact solution is 37.04^o). In the isotropic case, $\psi^I = \theta^I$ for all incident rays. ♣

Proposition 5: There is an incidence angle θ_3^I such that the propagation direction of the reflected wave coincides with the corresponding Umov-Poynting vector direction, i.e., $\theta^R = \psi^R$. From equations (6.44) and (6.55), we note that this proposition is verified when

$$\frac{\mathrm{Re}(s_1)}{\mathrm{Re}(s_3^R)} = \frac{\mathrm{Re}(X^R)}{\mathrm{Re}(Z^R)}. \tag{6.65}$$

The solutions are $\theta_3^I = 26.74^o$ and $\theta^R = -53.30^o$.

In the elastic case,

$$\tan\theta_3^I = (-b - \sqrt{b^2 - 4ac})/(2a), \tag{6.66}$$

where

$$a = c_{46}\left(\frac{2d}{c_{44}^2} - 1\right), \qquad b = \frac{c_{44}}{c_{46}}a - c_{66}, \qquad c = -c_{46}, \tag{6.67}$$

with

$$d = c_{44}c_{66} - 2c_{46}^2. \tag{6.68}$$

The corresponding reflection angle is obtained from equations (6.44) and (6.55), and given by

$$\tan\theta_3^R = \left[c_{66} - c_{44} + \sqrt{(c_{66} - c_{44})^2 + 4c_{46}^2}\right]/(2c_{46}). \tag{6.69}$$

The solutions are $\theta_3^I = 27.61^o$ and $\theta_3^R = -52.19^o$. In the isotropic case, $\psi^R = \theta^R$ for all incident rays. ♣

Proposition 6: An incident wave whose energy-flux vector is parallel to the interface ($\mathrm{Re}(Z^I) = 0$, see (6.9)) generates a reflected wave whose energy-flux vector is parallel to the interface ($\mathrm{Re}(Z^R) = 0$). Moreover, in the lossless case and beyond the critical angle, the energy-flux vector of the transmitted wave is parallel to the interface, i.e., $\mathrm{Re}(Z^T) = 0$.

This first statement can be deduced from equation (6.36). Moreover, from equations (6.39) and (6.41) ,

$$Z^T = \mathrm{pv}\sqrt{\rho' c'_{44} - c'^2 s_1^2}. \tag{6.70}$$

Beyond the critical angle, the horizontal slowness s_1 is greater than $\sqrt{\rho' c'_{44}}/c'$, where $c' = c'_{44}c'_{66} - c'^2_{46}$. Therefore, the quantity inside the square root becomes negative and $\mathrm{Re}(Z^T) = 0$. ♣

6.1.5 Brewster and critical angles

In 1815, David Brewster, basing his observations on an experiment by Malus, noted the existence of an angle (θ_B) such that: *if light is incident under this angle, the electric vector of the reflected light has no component in the plane of incidence* (Born and Wolf, 1964, p. 43). When this happens, $\theta_B + \theta^T = 90^o$ and the reflection coefficient of the wave with the electric vector in the plane of incidence vanishes. Here, we define the Brewster angle as the incidence angle for which $R_{SS} = 0$ (in elastodynamics, $\theta_B + \theta^T \neq 90^o$ in general).

From equation (6.34), this occurs when $Z^I = Z^T$, or from (6.10), when

$$p_{46}s_1 + p_{44}s_3^I = p'_{46}s_1 + p'_{44}s_3^T. \tag{6.71}$$

Using (6.27), (6.28) and (6.39), we see that equation (6.71) yields the following solution

$$\cot\theta_B = \left(-b \pm \mathrm{pv}\sqrt{b^2 - 4ac}\right)/(2a), \tag{6.72}$$

where

$$a = p_{44}(\rho p_{44} - \rho' p'_{44})/\rho, \qquad b = 2p_{46}a/p_{44}, \tag{6.73}$$

and

$$c = p_{46}^2 - {p'_{46}}^2 - p'_{44}(\rho' p_{66} - \rho p'_{66})/\rho. \tag{6.74}$$

In general, $\cot\theta_B$ is complex and there is no Brewster angle. In the elastic limit of the example, the Brewster angle is $\theta_B = 32.34^o$ (see Figure 6.5).

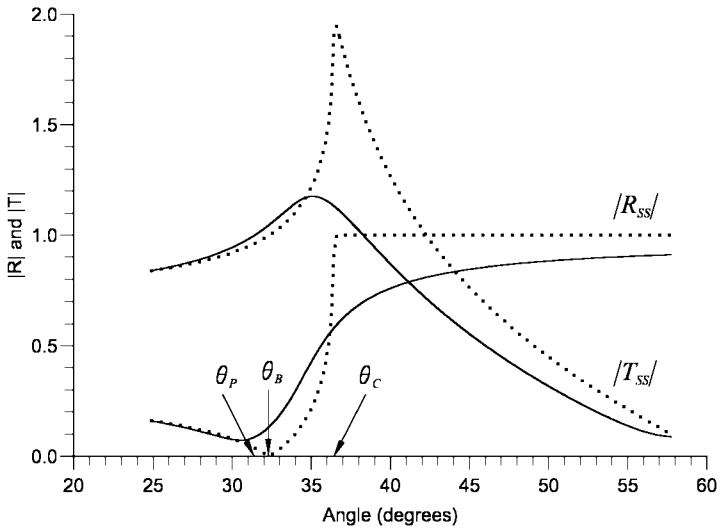

Figure 6.5: Absolute values of the reflection and transmission coefficients versus the incidence angle for the elastic (dotted line) and viscoelastic (solid line) cases (θ_P= 31.38°, θ_B = 32.34° and θ_C= 36.44°).

In the isotropic viscoelastic case, the solution is

$$\cot\theta_B = \pm\mathrm{pv}\sqrt{\frac{\rho' - \rho\mu'/\mu}{\rho\mu/\mu' - \rho'}}, \tag{6.75}$$

which is generally complex. The Brewster angle exists only in rare instances. For example, $\cot\theta_B$ is real for $\mathrm{Im}(\mu/\mu')$=0. In isotropic media, the complex velocity (6.28) is simply $v_c = \sqrt{\mu/\rho}$. Thus, the quality factor (4.92) for homogeneous waves in isotropic media is $Q = Q_H = \mathrm{Re}(\mu)/\mathrm{Im}(\mu)$. The condition $\mathrm{Im}(\mu/\mu') = 0$ implies that the Brewster angle exists when $Q_H = Q'_H$, where $Q'_H = \mathrm{Re}(\mu')/\mathrm{Im}(\mu')$.

In the lossless case and when $\rho = \rho'$, the reflected and transmitted rays are perpendicular to each other at the Brewster angle, i.e., $\theta_B + \theta^T = 90^o$. This property can be proved by using Snell's law and equation (6.75) (this exercise is left to the reader). On

the basis of the acoustic-electromagnetic mathematical analogy (Carcione and Cavallini, 1995b), the magnetic permeability is equivalent to the material density and the dielectric permittivity is equivalent to the reciprocal of the shear modulus (see Chapter 8). There is then a complete analogy between the reflection-transmission problem for isotropic, lossless acoustic media of equal density and the same problem in electromagnetism, where the media have zero conductivity and their magnetic permeability are similar (perfectly transparent media, see Born and Wolf (1964, p. 38)).

In anisotropic media, two singular angles can be defined depending on the orientation of both the propagation and the Umov-Poynting vectors with respect to the interface. The pseudocritical angle θ_P is defined as the angle of incidence for which the transmitted slowness vector is parallel to the interface. In Auld (1990b, p. 9), the critical angle phenomenon is related to the condition $s_3^T = 0$, but, as we shall see below, this is only valid when the lower medium has $p'_{46} = 0$ (e.g., transversely isotropic). The correct interpretation was given by Henneke II (1971), who defined the critical angle θ_C as the angle(s) of incidence beyond which the Umov-Poynting vector of the transmitted wave is parallel to the interface (see also Rokhlin, Bolland and Adler (1986)). From equations (2.113), (6.9) and (6.10), this is equivalent to $\mathrm{Re}(Z^T) = 0$. We keep the same interpretation for viscoelastic media. Actually, the pseudocritical angle does not play any important physical role in the anisotropic case.

The condition $\mathrm{Re}(Z^T)$=0 in equation (6.56) yields the critical angle θ_C, because $\psi_T = \pi/2$. Using equation (6.10), this gives

$$\mathrm{Re}(p'_{46}s_1 + p'_{44}s_3^T) = 0, \tag{6.76}$$

or, from (6.39) and (6.41),

$$\mathrm{Re}\left(\mathrm{pv}\sqrt{\rho' p'_{44} - p'^2 s_1^2}\right) = 0. \tag{6.77}$$

Since for a complex number q, it is $[\mathrm{Re}(\sqrt{q})]^2 = [|q| + \mathrm{Re}(q)]/2$, equation (6.77) is equivalent to

$$\mathrm{Im}(\rho' p'_{44} - p'^2 s_1^2) = 0. \tag{6.78}$$

For the particular case when $\rho' p'_{44} - p'^2 s_1^2 = 0$ and using (6.28), the following explicit solution is obtained:

$$\cot\theta_C = \frac{1}{p_{44}}\left(-p_{46} + \mathrm{pv}\sqrt{\frac{\rho p_{44}}{\rho' p'_{44}}p'^2 - p^2}\right). \tag{6.79}$$

There is a solution if the right-hand side of equation (6.79) is real. This occurs only in very particular situations.

In the isotropic case (see (6.25)), a critical angle exists if

$$\cot\theta_C = \sqrt{\frac{\rho}{\rho'}\frac{\mu'}{\mu} - 1} \tag{6.80}$$

is a real quantity. This is verified for μ'/μ real or $Q_H = Q'_H$ and $\rho\mu' > \rho'\mu$. Then, $\mu'/\mu = \mathrm{Re}(\mu')/\mathrm{Re}(\mu)$ and

$$\sin\theta_P = \sqrt{\frac{\rho'\mathrm{Re}(\mu)}{\rho\mathrm{Re}(\mu')}} = \sin\theta_C \tag{6.81}$$

(Borcherdt, 1977). The last equality holds since $p'_{46} = 0$ implies $\mathrm{Re}(s_3^T) = 0$ from equation (6.76).

Figure 6.5 shows the absolute values of the reflection and transmission coefficients versus the incidence angle for the elastic (dotted line) and viscoelastic (solid line) cases, respectively, with θ_P= 31.38°, θ_B = 32.34° and θ_C= 36.44°. The directions of the slowness and Umov-Poynting vectors, corresponding to the critical angle θ_C, can be appreciated in Figure 6.6, which illustrates the elastic case.

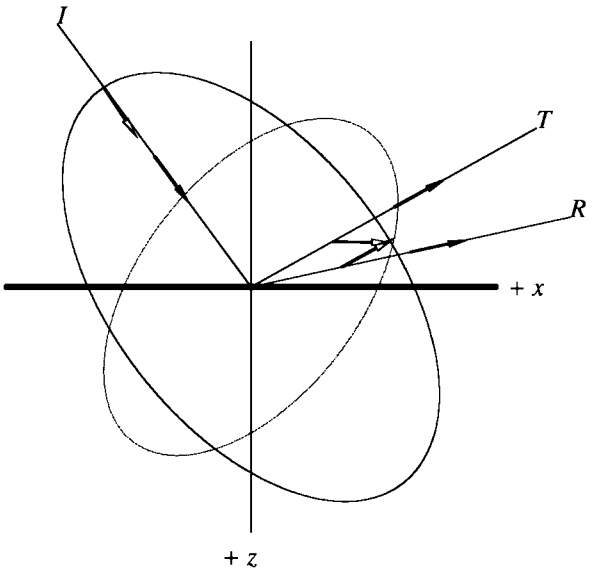

Figure 6.6: Directions of the slowness and Umov-Poynting vectors, corresponding to the critical angle θ_C = 36.44° for the elastic case. At the critical angle and beyond, the Umov-Poynting vector of the transmitted wave is parallel to the interface. Moreover, the transmitted wave becomes evanescent.

According to Proposition 6, at the critical angle and beyond, the Umov-Poynting vector of the transmitted wave is parallel to the interface and the wave becomes evanescent. A geometrical interpretation is that, in the elastic case, critical angles are associated with tangent planes to the slowness surface that are normal to the interface (see Figure 6.6). Snell's law requires that the end points of all the slowness vectors lie in a common normal line to the interface. We get the critical angle when this line is tangent to the slowness curve of the transmission medium. Beyond the critical angle, there is no intersection between that line and the slowness curve, and the wave becomes evanescent (Henneke II, 1971; Rokhlin, Bolland and Adler, 1986; Helbig 1994, p. 241).

In the lossless case, the Umov-Poynting vector is parallel to the boundary beyond the critical angle. Moreover, since Z^T is purely imaginary, equations (6.39) and (6.70) imply that $\mathrm{Re}(s_3^T) = -c'_{46}s_1/c'_{44}$. Finally, using equation (6.47), we obtain the propagation angle of the transmitted wave, namely,

$$\theta^T = -\arctan(c'_{44}/c'_{46}). \tag{6.82}$$

This angle takes the value $\theta^T = 119.75^o$ ($\psi^T = 90^o$) and remains constant for $\theta^I \geq \theta_C$. This phenomenon does not occur in the anelastic case.

As can be seen in Figure 6.5, there is no critical angle in the viscoelastic case and the reflection coefficient is always greater than zero (no Brewster angle). As in the isotropic case (Borcherdt, 1977), critical angles exist under very particular conditions.

Theorem 3: If one of the media is elastic and the other is anelastic, then there are no critical angles.

Proof: Suppose there exists a critical angle; that is, the Umov-Poynting vector of the transmitted wave is parallel to the interface. Assume first that the incidence medium is elastic. Proposition 1 implies that the attenuation of the transmitted wave is normal to the interface. However, since the transmission medium is anelastic, such an inhomogeneous wave – associated with elastic media – cannot propagate, otherwise $\langle D^T \rangle = 0$ (see equation (6.51)).

Conversely, assume a homogeneous plane wave, non-normal incidence and that the transmission medium is elastic. Since the incidence medium is anelastic, Snell's law requires a transmitted inhomogeneous wave of the viscoelastic type ($\boldsymbol{\alpha} \cdot \langle \mathbf{p} \rangle \neq 0$) in the transmission medium. However, this wave cannot propagate in an elastic medium (see equation (6.51)). ♣

A special case: Let us consider that both media are transversely isotropic and that $M_2 = M_1' = M_2' = M_1$. This case is similar to the one studied by Krebes (1983b) in isotropic media. Equation (6.78) gives the solution

$$\cot \theta_C = \sqrt{\frac{\rho c_{66}'}{\rho' c_{44}} - \frac{c_{66}}{c_{44}}} \tag{6.83}$$

and $s_1 = \sqrt{\rho'/p_{66}'}$, which implies $s_3^T = 0$. The critical angle for this case is $\theta_C = 47.76^o$. It can be shown from equations (6.27), (6.32), (6.34), (6.35) and (6.39) that the reflection and transmission coefficients are identical to those for perfect elasticity. However, beyond the critical angle, there is a normal interference flux (see Section 6.1.7) towards the boundary, complemented by a small energy flow away from the boundary in the transmission medium. This means that θ_C is a "discrete critical angle", i.e., the Umov-Poynting vector of the transmitted wave is parallel to the boundary only for the incidence angle θ_C. (In the elastic case this happens for $\theta^I \geq \theta_C$.) Since $s_3^T = 0$ at the critical angle, this occurs when the normal to the interface with abscissa $\mathrm{Re}(s_1)$ is tangent to the slowness curve of the transmitted wave and, simultaneously, the normal to the interface with abscissa $\mathrm{Im}(s_1)$ is tangent to the attenuation curve of the same wave.

6.1.6 Phase velocities and attenuations

The magnitude of the phase velocities can be obtained as the reciprocal of the slownesses. From equations (6.2) and (6.27), the phase velocity of the incident wave is simply

$$v_p^I = \{[\mathrm{Re}(s_1)]^2 + [\mathrm{Re}(s_3^I)]^2\}^{-1/2} = \left[\mathrm{Re}(v_c^{-1})\right]^{-1}. \tag{6.84}$$

The phase velocity of the reflected wave is obtained from equation (6.30) and written as

$$v_p^R = \{[\mathrm{Re}(s_1)]^2 + [\mathrm{Re}(s_3^R)]^2\}^{-1/2}, \tag{6.85}$$

or, using equations (6.10), (6.27) and (6.35), as

$$v_p^R = \left\{(v_p^I)^{-2} + 4\sin(\theta^I)\mathrm{Re}\left(p_{46}p_{44}^{-1}v_c^{-1}\right)\mathrm{Re}(p_{44}^{-1}Z^I)\right\}^{-1/2}. \tag{6.86}$$

When the Umov-Poynting vector of the incident wave is parallel to the interface ($Z^I = 0$), or when the upper medium is transversely isotropic ($p_{46} = 0$), v_p^R equals v_p^I. In the elastic case, equation (6.86) reduces to

$$v_p^R = v_p^I\{1 + 4\sin(\theta^I)c_{46}c_{44}^{-1}[c_{46}c_{44}^{-1}\sin\theta^I + \cos\theta^I]\}^{-1/2}. \tag{6.87}$$

Similarly, the phase velocity of the transmitted wave is obtained from equation (6.31) and written as

$$v_p^T = \{[\mathrm{Re}(s_1)]^2 + [\mathrm{Re}(s_3^T)]^2\}^{-1/2}. \tag{6.88}$$

The phase velocities of the incident, reflected and transmitted waves, versus the incidence angle, are represented in Figure 6.7, where the dotted line corresponds to the elastic case. The velocity in the elastic case is always higher than the velocity in the viscoelastic case, since the former case is taken at the high-frequency limit.

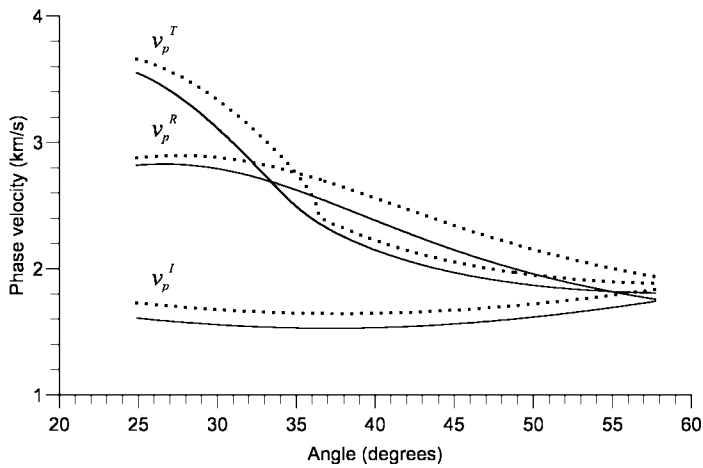

Figure 6.7: Phase velocities of the incident, reflected and transmitted waves versus the incidence angle. The elastic case is represented by a dotted line.

By virtue of equations (6.3), (6.27) and (6.30), the magnitudes of the attenuation vectors of the incident and reflected waves are given by

$$\alpha^I = \omega\sqrt{[\mathrm{Im}(s_1)]^2 + [\mathrm{Im}(s_3^I)]^2} = -\omega\mathrm{Im}(v_c^{-1}) \tag{6.89}$$

and

$$\alpha^R = \omega\sqrt{[\mathrm{Im}(s_1)]^2 + [\mathrm{Im}(s_3^R)]^2} \tag{6.90}$$

or, using equations (6.10), (6.27) and (6.35),

$$\alpha^R = \sqrt{(\alpha^I)^2 + 4\omega^2\sin(\theta)\mathrm{Im}\left(p_{46}p_{44}^{-1}v_c^{-1}\right)\mathrm{Im}(p_{44}^{-1}Z^I)}. \tag{6.91}$$

In the transversely isotropic case ($p_{46} = 0$), $\alpha^R = \alpha^I$. The magnitude of the attenuation vector of the transmitted wave is obtained from equation (6.31), and written as

$$\alpha^T = \omega\sqrt{[\mathrm{Im}(s_1)]^2 + [\mathrm{Im}(s_3^T)]^2}. \tag{6.92}$$

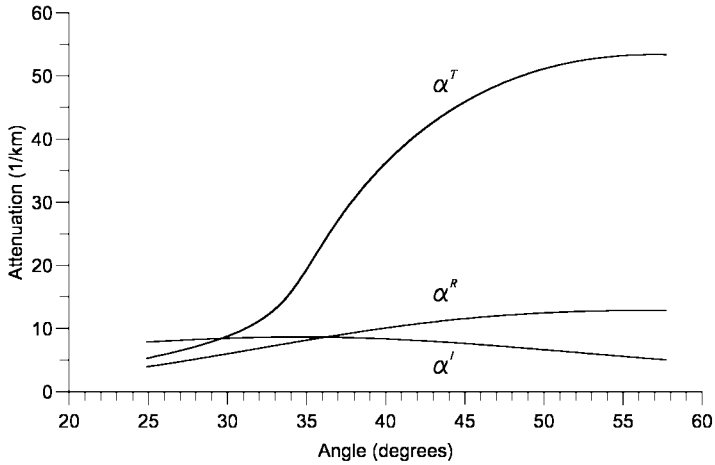

Figure 6.8: Attenuations of the incident, reflected and transmitted waves versus the incidence angle.

The attenuations are represented in Figure 6.8. The high attenuation value of the transmitted wave can be explained as follows. Figure 6.3 indicates that, at approximately the elastic-case critical angle and beyond, the energy angle of the transmitted wave ψ^T is close to $\pi/2$ and that the attenuation vector is almost perpendicular to the interface. In practice, this implies that the transmitted wave resembles an evanescent wave of the elastic type. This effect tends to disappear when the intrinsic quality factors of the lower and/or upper media are lower than the values given in Section 6.1.2.

6.1.7 Energy-flux balance

In order to balance energy flux at an interface between two isotropic single-phase media, it is necessary to consider the interaction energy fluxes when the media are viscoelastic (Borcherdt, 1977; Krebes, 1983b). In the incidence medium, for instance, the interaction energy fluxes arise from the interaction of the stress and velocity fields of the incident and reflected waves. A similar phenomenon takes place at an interface separating two porous media when the fluid viscosity is different from zero. Dutta and Odé (1983) call these fluxes interference fluxes and show that they vanish for zero viscosity.

In a welded interface, the normal component of the average Umov-Poynting $\hat{\mathbf{e}}_3 \cdot \langle \mathbf{p} \rangle$ is continuous across the interface. This is a consequence of the boundary conditions that impose continuity of normal stress σ_{32}, and particle velocity. Then, according to equation (4.111), the balance of power flow at the interface can be expressed as

$$-\frac{1}{2}\mathrm{Re}[(\sigma_{32}^I + \sigma_{32}^R)(v^I + v^R)^*] = -\frac{1}{2}\mathrm{Re}(\sigma_{32}^T v^{T*}). \tag{6.93}$$

Using equations (6.9) and (6.36), equation (6.93) is of the form

$$\langle p_3^I \rangle + \langle p_3^R \rangle + \langle p_3^{IR} \rangle = \langle p_3^T \rangle, \tag{6.94}$$

where

$$\langle p_3^I \rangle = -\frac{1}{2}\mathrm{Re}(\sigma_{32}^I v^{I^*}) = \frac{1}{2}\omega^2 \mathrm{Re}(Z^I)\exp[2\omega \mathrm{Im}(s_1)x] \tag{6.95}$$

is the flux of the incident wave,

$$\langle p_3^R \rangle = -\frac{1}{2}\mathrm{Re}(\sigma_{32}^R v^{R^*}) = \frac{1}{2}\omega^2 |R_{\mathrm{SS}}|^2 \mathrm{Re}(Z^R)\exp[2\omega \mathrm{Im}(s_1)x] \tag{6.96}$$

is the reflected flux,

$$\begin{aligned}\langle p_3^{IR} \rangle &= -\frac{1}{2}\mathrm{Re}(\sigma_{32}^I v^{R^*} + \sigma_{32}^R v^{I^*}) = \frac{1}{2}\omega^2 (Z^I R_{\mathrm{SS}}^* + Z^R R_{\mathrm{SS}})\exp[2\omega \mathrm{Im}(s_1)x] \\ &= \omega^2 \mathrm{Im}(R_{\mathrm{SS}})\mathrm{Im}(Z^I)\exp[2\omega \mathrm{Im}(s_1)x]\end{aligned} \tag{6.97}$$

is the interference between the normal fluxes of the incident and reflected waves, and

$$\langle p_3^T \rangle = -\frac{1}{2}\mathrm{Re}(\sigma_{32}^T v^{T^*}) = \frac{1}{2}\omega^2 |T_{\mathrm{SS}}|^2 \mathrm{Re}(Z^T)\exp[2\omega \mathrm{Im}(s_1)x] \tag{6.98}$$

is the flux of the transmitted wave. In the elastic case, Z^I is real and the interference flux vanishes.

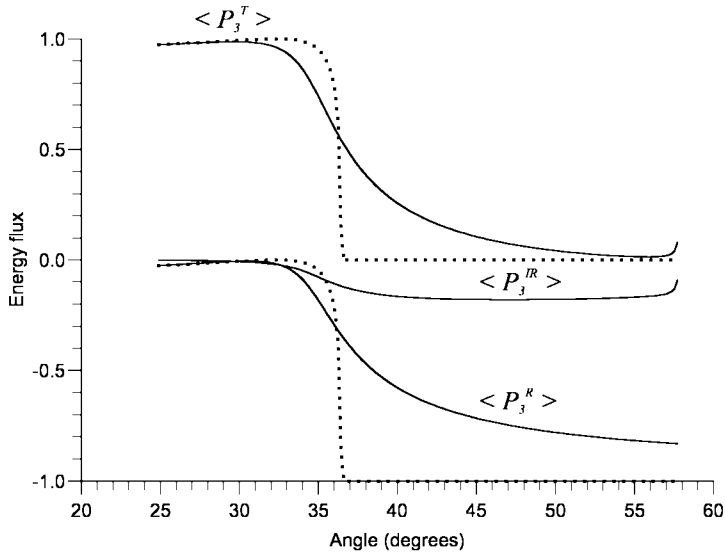

Figure 6.9: Normalized fluxes (energy coefficients) versus the incidence angle. The fluxes are normalized with respect to the flux of the incident wave. The elastic case is represented by a dotted line.

The normalized normal fluxes (energy coefficients) versus the incidence angle are shown in Figures 6.9, with the dotted line representing the elastic case. Beyond the

critical angle, the normal component of the Umov-Poynting vector of the transmitted wave vanishes and there is no transmission to the lower medium. The energy travels along the interface and, as stated before, the plane wave is evanescent. In the viscoelastic case, these effects disappear and the fluxes of the reflected and transmitted waves have to balance with a non-zero interference flux. Since the flux of the transmitted wave is always greater than zero, there is transmission for all the incidence angles.

6.1.8 Energy velocities and quality factors

The energy velocity $\mathbf{v}_e$ is the ratio of the average power-flow density $\langle \mathbf{p} \rangle = \mathrm{Re}(\mathbf{p})$ to the mean energy density $\langle T + V \rangle$ (see equation (4.76)). For the incident homogeneous wave, substitution of (6.27) into (6.16) and use of (6.28) gives $\varrho^I = \rho v_c^2/|v_c|^2$. Then, equations (6.14) and (6.17) imply

$$\langle T + V \rangle = \frac{1}{4}\rho\omega^2 \left[\frac{\mathrm{Re}(v_c^2)}{|v_c|^2} + 1 \right] \exp\{2\omega[\mathrm{Im}(s_1)x + \mathrm{Im}(s_3^I)z]\}. \tag{6.99}$$

Using the relation $[\mathrm{Re}(v_c)]^2 = [|v_c|^2 + \mathrm{Re}(v_c^2)]/2$, equation (6.99) becomes

$$\langle T + V \rangle = \frac{1}{2}\rho\omega^2 (v_p^I)^{-1} \exp\{2\omega[\mathrm{Im}(s_1)x + \mathrm{Im}(s_3^I)z]\}\ \mathrm{Re}(v_c), \tag{6.100}$$

where v_p^I is the phase velocity (6.84). Finally, combining (6.9) and (6.100), we obtain

$$\mathbf{v}_e^I = \frac{v_p^I}{\rho \mathrm{Re}(v_c)} \mathrm{Re}(X^I \hat{\mathbf{e}}_1 + Z^I \hat{\mathbf{e}}_3). \tag{6.101}$$

The energy velocity of the reflected wave is obtained from equations (6.9), (6.14), (6.16) and (6.17), and written as

$$\mathbf{v}_e^R = \frac{2\mathrm{Re}(X^R \hat{\mathbf{e}}_1 + Z^R \hat{\mathbf{e}}_3)}{\rho + \mathrm{Re}(\varrho^R)}, \tag{6.102}$$

where $\varrho^R = \varrho(s_3^R)$. If the upper medium has $p_{46} = 0$ (e.g., transverse isotropy), $X^R = X^I$ and $\varrho^R = \rho v_c^2/|v_c|^2$. After some algebra, it can be shown, using (6.35) and (6.36), that $v_e^R = v_e^I$.

Similarly, the energy velocity of the transmitted wave is

$$\mathbf{v}_e^T = \frac{2\mathrm{Re}(X^T \hat{\mathbf{e}}_1 + Z^T \hat{\mathbf{e}}_3)}{\rho' + \mathrm{Re}(\varrho^T)}, \tag{6.103}$$

where $\varrho^T = \varrho(s_3^T)$.

An alternative expression for the energy velocity is obtained from the fact that, as in the elastic case, the phase velocity is the projection of the energy-velocity vector onto the propagation direction. This relation is demonstrated in Section 4.3.1 (equation (4.78)) for inhomogeneous waves propagating in a general anisotropic viscoelastic medium. For cross-plane shear waves, we have

$$v_e = v_p / \cos(\psi - \theta). \tag{6.104}$$

In terms of the tangents defined in Section 6.1.4,

$$v_e = \left[\frac{\sqrt{(1+\tan^2\psi)(1+\tan^2\theta)}}{(1+\tan\psi\tan\theta)} \right] v_p. \tag{6.105}$$

The energy velocities of the incident, reflected and transmitted waves, versus the incidence angle, are represented in Figures 6.10, with the dotted line corresponding to the elastic case.

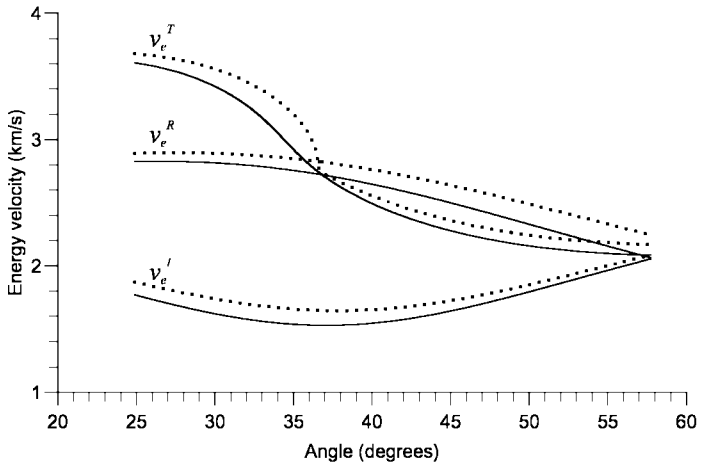

Figure 6.10: Energy velocities of the incident, reflected and transmitted waves, versus the incidence angle. The elastic case is represented by a dotted line.

Comparison of Figures 6.7 and 6.10 indicates that the energy velocity in anisotropic viscoelastic media is greater or equal than the phase velocity – as predicted by equation (6.104).

The quality factor is the ratio of twice the average strain-energy density (6.14) to the dissipated-energy density (6.15). For the incident homogeneous wave it is simply

$$Q_H^I = \frac{\mathrm{Re}(\varrho^I)}{\mathrm{Im}(\varrho^I)} = \frac{\mathrm{Re}(v_c^2)}{\mathrm{Im}(v_c^2)}, \tag{6.106}$$

while for the reflected and transmitted waves,

$$Q^R = \frac{\mathrm{Re}(\varrho^R)}{\mathrm{Im}(\varrho^R)} \tag{6.107}$$

and

$$Q^T = \frac{\mathrm{Re}(\varrho^T)}{\mathrm{Im}(\varrho^T)}, \tag{6.108}$$

respectively. When $p_{46} = 0$ and using (6.35), $\varrho^R = \rho v_c^2/|v_c|^2$, and Q^R equals Q^I.

Let us consider the incident homogeneous wave. From equation (6.28), $\rho v_c^2 = p_{44}$ along the z-axis. Substitution of (6.18) into (6.106) and the use of (6.19) gives equation (6.21). Then, the quality factor along the vertical direction is Q_{01} at the reference frequency f_0. Similarly, it can be shown that Q_{02} is the quality factor along the horizontal direction.

In Chapter 8, we demonstrate that the equations describing propagation of the TM (transverse magnetic) mode in a conducting anisotropic medium are completely analogous – from the mathematical point of view – to the propagation of viscoelastic cross-plane shear waves in the plane of symmetry of a monoclinic medium. This equivalence identifies the magnetic field with the particle velocity, the electric field with the stress components, and the compliance components p_{IJ}^{-1} with the complex dielectric-permittivity components. Therefore, the present reflection-transmission analysis can be applied to the electromagnetic case with minor modifications.

6.2 Reflection and transmission of qP-qSV waves

A review of the literature pertaining to the reflection-transmission problem in anisotropic elastic media and isotropic viscoelastic media is given in Sections 1.9 and 3.8, respectively. The time-domain equations for propagation in a heterogeneous viscoelastic transversely isotropic medium are given in Chapter 4, Section 4.5.

6.2.1 Propagation characteristics

A general plane-wave solution for the particle-velocity field $\mathbf{v} = (v_1, v_3)$ is

$$\mathbf{v} = \mathrm{i}\omega \mathbf{U} \exp\left[\mathrm{i}\omega(t - s_1 x - s_3 z)\right], \tag{6.109}$$

where s_1 and s_3 are the components of the complex-slowness vector, and $\mathbf{U}$ is a complex vector. The real-valued slowness and attenuation vectors are given by

$$\mathbf{s}_R = (\mathrm{Re}(s_1), \mathrm{Re}(s_3)) \tag{6.110}$$

and

$$\boldsymbol{\alpha} = -\omega(\mathrm{Im}(s_1), \mathrm{Im}(s_3)), \tag{6.111}$$

respectively. The complex-slowness vector is then

$$\mathbf{s} = \mathbf{s}_R - \frac{\mathrm{i}\boldsymbol{\alpha}}{\omega}, \qquad s^2 = s_1^2 + s_3^2. \tag{6.112}$$

The dispersion relation can be obtained from equation $(1.78)_2$, by using (1.74), $s_1 = sl_1$, $s_3 = sl_3$, and the correspondence principle ((Section 3.6) ($c_{IJ} \to p_{IJ}$)). Hence, we have

$$F(s_1, s_3) = (p_{11}s_1^2 + p_{55}s_3^2 - \rho)(p_{33}s_3^2 + p_{55}s_1^2 - \rho) - (p_{13} + p_{55})^2 s_1^2 s_3^2 = 0, \tag{6.113}$$

which has two solutions corresponding to the quasi-compressional (qP) and quasi-shear (qS) waves. The form (6.113) holds for inhomogeneous plane waves in viscoelastic media.

Let us assume that the positive z-axis points downwards. In order to distinguish between down and up propagating waves, the slowness relation equation (6.113) is solved for s_3, given the horizontal slowness s_1. This yields

$$s_3 = \pm\frac{1}{\sqrt{2}}\sqrt{K_1 \mp \mathrm{pv}\sqrt{K_1^2 - 4K_2K_3}}, \tag{6.114}$$

where

$$K_1 = \rho\left(\frac{1}{p_{55}} + \frac{1}{p_{33}}\right) + \frac{1}{p_{55}}\left[\frac{p_{13}}{p_{33}}(p_{13} + 2p_{55}) - p_{11}\right]s_1^2,$$

$$K_2 = \frac{1}{p_{33}}(p_{11}s_1^2 - \rho), \qquad K_3 = s_1^2 - \frac{\rho}{p_{55}}.$$

The signs in s_3 correspond to

$(+,-)$	downward propagating qP wave
$(+,+)$	downward propagating qS wave
$(-,-)$	upward propagating qP wave
$(-,+)$	upward propagating qS wave.

The plane-wave eigenvectors (polarizations) belonging to a particular eigenvalue can be obtained from the qP-qS Kelvin-Christoffel equation by using equation (1.81) and the correspondence principle. We obtain

$$\mathbf{U} = U_0\begin{pmatrix}\beta\\ \xi\end{pmatrix}, \tag{6.115}$$

where U_0 is the plane-wave amplitude and

$$\beta = \mathrm{pv}\sqrt{\frac{p_{55}s_1^2 + p_{33}s_3^2 - \rho}{p_{11}s_1^2 + p_{33}s_3^2 + p_{55}(s_1^2 + s_3^2) - 2\rho}} \tag{6.116}$$

and

$$\xi = \pm\mathrm{pv}\sqrt{\frac{p_{11}s_1^2 + p_{55}s_3^2 - \rho}{p_{11}s_1^2 + p_{33}s_3^2 + p_{55}(s_1^2 + s_3^2) - 2\rho}}. \tag{6.117}$$

In general, the $+$ and $-$ signs correspond to the qP and qS waves, respectively. However one must choose the signs such that ξ varies smoothly with the propagation angle. In the elastic case, the qP eigenvectors are orthogonal to the qS eigenvectors only when the respective slownesses are parallel. In the viscoelastic case, this property is not satisfied. From equations (6.109), (6.116) and (6.117), and using (6.110) and (6.111), the particle-velocity field can be written as

$$\mathbf{v} = \mathrm{i}\omega U_0\begin{pmatrix}\beta\\ \xi\end{pmatrix}\exp\{\omega[\mathrm{Im}(s_1)x + \mathrm{Im}(s_3)z]\}\exp\{\mathrm{i}\omega[t - \mathrm{Re}(s_1)x - \mathrm{Re}(s_3)z]\}. \tag{6.118}$$

The mean flux or time-averaged Umov-Poynting vector $\langle\mathbf{p}\rangle$ is the real part of the corresponding complex vector (see equation (4.55)),

$$\mathbf{p} = -\frac{1}{2}[(\sigma_{11}v_1^* + \sigma_{13}v_3^*)\hat{\mathbf{e}}_1 + (\sigma_{13}v_1^* + \sigma_{33}v_3^*)\hat{\mathbf{e}}_3]. \tag{6.119}$$

Substituting the plane wave (6.118) and the stress-strain relation (4.160) into equation (6.119), we obtain

$$\mathbf{p} = \frac{1}{2}\omega^2|U_0|^2 \begin{pmatrix} \beta^* X + \xi^* W \\ \beta^* W + \xi^* Z \end{pmatrix} \exp\{2\omega[\mathrm{Im}(s_1)x + \mathrm{Im}(s_3)z]\}, \tag{6.120}$$

where

$$W = p_{55}(\xi s_1 + \beta s_3), \tag{6.121}$$

$$X = \beta p_{11} s_1 + \xi p_{13} s_3, \tag{6.122}$$

$$Z = \beta p_{13} s_1 + \xi p_{33} s_3 \tag{6.123}$$

and the strain-displacement relations (1.2) have been used.

6.2.2 Properties of the homogeneous wave

For homogeneous waves, the directions of propagation and attenuation coincide and

$$s_1 = \sin\theta/v_c(\theta), \quad s_3 = \cos\theta/v_c(\theta), \tag{6.124}$$

where θ is the propagation angle, measured with respect to the z-axis, and $v_c = 1/s$ is the complex velocity that can be obtained from the slowness relation (6.113). Hence, we have

$$\rho v_c^2 = \frac{1}{2}(p_{55} + p_{11}\sin^2\theta + p_{33}\cos^2\theta \pm C), \tag{6.125}$$

with

$$C = \sqrt{[(p_{33} - p_{55})\cos^2\theta - (p_{11} - p_{55})\sin^2\theta]^2 + (p_{13} + p_{55})^2 \sin^2 2\theta}. \tag{6.126}$$

The + sign corresponds to the qP wave, and the − sign to the qS wave.

Combining (6.110), (6.111) and (6.124) yields

$$\mathbf{s}_R = \mathrm{Re}\left(\frac{1}{v_c}\right)(\sin\theta, \cos\theta), \tag{6.127}$$

and

$$\boldsymbol{\alpha} = -\omega \mathrm{Im}\left(\frac{1}{v_c}\right)(\sin\theta, \cos\theta). \tag{6.128}$$

The quality factor is

$$Q = \frac{\mathrm{Re}(v_c^2)}{\mathrm{Im}(v_c^2)} \tag{6.129}$$

(see equation (4.92)). For instance, for model 3 (for the 2-D case, see Sections 4.1.3 and 4.5.4, equation (4.161)) we point out the following properties. At the symmetry axis ($\theta = 0$), for qP waves, $v_c^2 = \rho p_{33}$, and at the isotropy plane ($\theta = \pi/2$), $v_c^2 = \rho p_{11}$. Then, the relation between Q factors is

$$\frac{Q(\text{symmetry axis})}{Q(\text{isotropy plane})} = \frac{c_{33} - a}{c_{11} - a}, \quad a = \bar{\mathcal{E}} - \bar{\mathcal{K}}\mathrm{Re}(M_1) - c_{55}\mathrm{Re}(M_2). \tag{6.130}$$

We can verify that $a > 0$, $a < c_{11}$ and $a < c_{33}$, for most realistic materials – in the elastic case, $a = 0$ ($M_1 = M_2 = 0$, see equation (4.156)). This implies that, whatever the ratio c_{33}/c_{11}, the ratio between Q factors is farther from unity than the elastic-velocity ratio $\sqrt{c_{33}/c_{11}}$. It follows that attenuation is a better indicator of anisotropy than elastic velocity. Similarly, it can be shown that the ratio between the viscoelastic phase velocities $\mathrm{Re}(1/\sqrt{p_{11}})/\mathrm{Re}(1/\sqrt{p_{33}})$ is closer to one than the Q ratio.

Another important property is that, when $c_{11} > c_{33}$ (e.g., finely layered media, see Section 1.5), the qP wave attenuates more along the symmetry axis than in the plane of isotropy. Note that we do not use an additional relaxation function to model Q anisotropy of the qP wave. It is the structure of the medium – described by the stiffnesses – that dictates the Q ratio between different propagation directions.

On the other hand, the quality factor of the shear wave at the symmetry axis is equal to the quality factor in the plane of isotropy, since $v_c^2 = \rho p_{55}$ in both cases. This is so, since any kind of symmetry possessed by the attenuation should follow the symmetry of the crystallographic form of the material (Neumann's principle, see Nye, 1987, p. 20). A qS wave anisotropy factor can be defined as the ratio of the vertical phase velocity to the phase velocity at an angle of 45° to the axis of symmetry. Again, it can be shown that, for most realistic materials, this factor is closer to one than the ratio between the respective quality factors.

6.2.3 Reflection and transmission coefficients

The upper layer is denoted by the subscript 1 and the lower layer by the subscript 2. For clarity, the material properties of the lower medium are primed and the symbols P and S indicate the qP and qS waves, respectively. Moreover, the subscripts I, R and T denote the incident, reflected and transmitted waves. Using symmetry properties to define the polarization of the reflected waves, the particle velocities for a qP wave incident from above the interface are given by

$$\mathbf{v}_1 = \mathbf{v}_{P_I} + \mathbf{v}_{P_R} + \mathbf{v}_{S_R}, \tag{6.131}$$

$$\mathbf{v}_2 = \mathbf{v}_{P_T} + \mathbf{v}_{S_T}, \tag{6.132}$$

where

$$\mathbf{v}_{P_I} = \mathrm{i}\omega(\beta_{P_1}, \xi_{P_1}) \exp\left[\mathrm{i}\omega(t - s_1 x - s_{3P_1} z)\right], \tag{6.133}$$

$$\mathbf{v}_{P_R} = \mathrm{i}\omega R_{\mathrm{PP}}(\beta_{P_1}, -\xi_{P_1}) \exp\left[\mathrm{i}\omega(t - s_1 x + s_{3P_1} z)\right], \tag{6.134}$$

$$\mathbf{v}_{S_R} = \mathrm{i}\omega R_{\mathrm{PS}}(\beta_{S_1}, -\xi_{S_1}) \exp\left[\mathrm{i}\omega(t - s_1 x + s_{3S_1} z)\right], \tag{6.135}$$

$$\mathbf{v}_{P_T} = \mathrm{i}\omega T_{\mathrm{PP}}(\beta_{P_2}, \xi_{P_2}) \exp\left[\mathrm{i}\omega(t - s_1 x - s_{3P_2} z)\right], \tag{6.136}$$

and

$$\mathbf{v}_{S_T} = \mathrm{i}\omega T_{\mathrm{PS}}(\beta_{S_2}, \xi_{S_2}) \exp\left[\mathrm{i}\omega(t - s_1 x - s_{3S_2} z)\right]. \tag{6.137}$$

The boundary conditions (continuity of the particle velocity and normal stress components) give Snell's law, i.e., the continuity of the horizontal complex slowness s_1. The vertical slownesses s_{3P} and s_{3S}, as well as β_P, β_S, ξ_P and ξ_S, follow respectively the $(+,-)$ and $(+,+)$ sign sets given in equation (6.114). The choice $U_0 = 1$ implies no loss of generality.

The boundary conditions require continuity of

$$v_1, \quad v_3, \quad \sigma_{33}, \quad \text{and} \quad \sigma_{13}. \tag{6.138}$$

The stresses are obtained by the substitution of equations (6.131) and (6.132) into the stress-strain relation (4.160). The boundary conditions generate the following matrix equation for the reflection and transmission coefficients:

$$\begin{pmatrix} \beta_{P_1} & \beta_{S_1} & -\beta_{P_2} & -\beta_{S_2} \\ \xi_{P_1} & \xi_{S_1} & \xi_{P_2} & \xi_{S_2} \\ Z_{P_1} & Z_{S_1} & -Z_{P_2} & -Z_{S_2} \\ W_{P_1} & W_{S_1} & W_{P_2} & W_{S_2} \end{pmatrix} \cdot \begin{pmatrix} R_{\mathrm{PP}} \\ R_{\mathrm{PS}} \\ T_{\mathrm{PP}} \\ T_{\mathrm{PS}} \end{pmatrix} = \begin{pmatrix} -\beta_{P_1} \\ \xi_{P_1} \\ -Z_{P_1} \\ W_{P_1} \end{pmatrix}, \tag{6.139}$$

where W and Z are given by equations (6.121) and (6.123), respectively.

The steps to compute the reflection and transmission coefficients are the following:

1. The horizontal slowness s_1 is the independent parameter. It is the same for all the waves (Snell's law for viscoelastic media). For an incident homogeneous wave, the independent variable becomes the incidence angle θ, and s_1 is obtained from equation (6.124).

2. Compute s_{3P_1}, s_{3S_1}, s_{3P_2} and s_{3S_2} from equation (6.114), where the first sign is positive. For an incident homogeneous wave, s_{3P_1} can be calculated either from equation (6.114) or from equation (6.124).

3. Compute β_{P_1}, β_{S_1}, β_{P_2}, β_{S_2}, ξ_{P_1}, ξ_{S_1}, ξ_{P_2} and ξ_{S_2} from equations (6.116) and (6.117).

4. Compute W_{P_1}, W_{S_1}, W_{P_2} and W_{S_2} from equation (6.121), and Z_{P_1}, Z_{S_1}, Z_{P_2} and Z_{S_2} from equation (6.123).

5. Compute the reflection and transmission coefficients by numerically solving equation (6.139).

The reflection and transmission coefficients R_{SP}, R_{SS}, T_{SP} and T_{SS} for an incident qS wave have the same 4×4 scattering matrix as the qP incident wave, but the vector in the right-hand side of (6.139) is

$$(-\beta_{S_1}, \xi_{S_1}, -Z_{S_1}, W_{S_1})^{\top}. \tag{6.140}$$

6.2.4 Propagation, attenuation and energy directions

Figure 6.1 illustrates the convention used to define the propagation, attenuation and energy angles. The propagation direction is perpendicular to the plane-wave front. Given the components of the complex-slowness vector, the propagation and attenuation angles for all the waves can be obtained and expressed as

$$\tan\theta = \frac{\mathrm{Re}(s_1)}{\mathrm{Re}(s_3)}, \quad \text{and} \quad \tan\delta = \frac{\mathrm{Im}(s_1)}{\mathrm{Im}(s_3)}. \tag{6.141}$$

By hypothesis (see equation (6.124)), $\delta_{P_I} = \theta_{P_I}$, and by symmetry, $\theta_{P_R} = -\theta_{P_I}$ and $\delta_{P_R} = \theta_{P_R}$. Hence, the reflected qP wave is homogeneous.

The complex vertical slowness component of the reflected qS wave is $-s_{3S_1}$, following the $(-,+)$ sign in equation (6.114). Then, the propagation and attenuation angles θ_{S_R} and δ_{S_R} are obtained from (6.141) with the substitution $s_3 = -s_{3S_1}$. In general $\theta_{S_R} \neq \delta_{S_R}$ and the wave is inhomogeneous. Analogously, the angles of the transmitted qP wave (θ_{P_T} and δ_{P_T}) and the transmitted qS wave (θ_{S_T} and δ_{S_T}) are given by (6.141) when $s_3 = s_{3P_2}$ and $s_3 = s_{3S_2}$, respectively. The transmitted waves are, in general, inhomogeneous.

The expressions of the time-averaged Umov-Poynting vectors of the reflected and transmitted waves are given by equation (6.120). Then, the angles of the energy vectors of the incident, reflected and transmitted waves are obtained from

$$\tan\psi = \frac{\mathrm{Re}(\beta^* X + \xi^* W)}{\mathrm{Re}(\beta^* W + \xi^* Z)}. \tag{6.142}$$

By symmetry, we have $\psi_{P_R} = -\psi_{P_I}$.

6.2.5 Phase velocities and attenuations

The magnitude of the phase velocities can be obtained as the reciprocal of the slownesses. From equation (6.110), the phase velocity of the incident and reflected waves is simply

$$v_p = \{[\mathrm{Re}(s_1)]^2 + [\mathrm{Re}(s_3)]^2\}^{-1/2}. \tag{6.143}$$

Since the incident wave is homogeneous, the use of equation (6.124) yields

$$v_{p_{P_I}} = \left[\mathrm{Re}(v_{c1}^{-1})\right]^{-1}, \tag{6.144}$$

where v_{c1} is the complex velocity for homogeneous waves in the incidence medium (equation (6.125)). By symmetry (see also Section 3.5), the phase velocity of the reflected qP wave $v_{p_{P_R}}$ equals $v_{p_{P_I}}$.

The velocities $v_{p_{S_R}}$, $v_{p_{P_T}}$ and $v_{p_{S_T}}$ are obtained from (6.143) by replacing s_3 by $-s_{3S_1}$, s_{3P_2} and s_{3S_2}, respectively.

The magnitude of the attenuation vectors is given by

$$\alpha = \omega\{[\mathrm{Im}(s_1)]^2 + [\mathrm{Im}(s_3)]^2\}^{-1/2}. \tag{6.145}$$

The incident and qP reflected waves have the same value:

$$\alpha_{P_I} = -\omega\ \mathrm{Im}(v_{c1}^{-1}), \tag{6.146}$$

while the attenuations α_{S_R}, α_{P_T} and α_{S_T} are obtained from (6.145) by replacing s_3 by $-s_{3S_1}$, s_{sP_2} and s_{3S_2}, respectively.

6.2.6 Energy-flow balance

We have seen in Section 6.1.7 that to balance energy flux at an interface between two isotropic single-phase media, it is necessary to consider the interaction energy fluxes when the media are viscoelastic. In the incidence medium, for instance, these fluxes arise from the interaction of the stress and particle-velocity fields of the incident and reflected waves.

In a welded interface, the normal component of the average Umov-Poynting $\hat{\mathbf{e}}_3 \cdot \langle \mathbf{p} \rangle$ is continuous across the interface. This is a consequence of the boundary conditions that impose continuity of normal stresses and particle velocities. Then, using equation (6.119), the balance of power flow implies the continuity of

$$-\frac{1}{2}\mathrm{Re}(\sigma_{13}v_1^* + \sigma_{33}v_3^*), \tag{6.147}$$

where each component is the sum of the components of the respective waves, e.g., $v_1 = v_{1P_I} + v_{1P_R} + v_{1S_R}$ in the incidence medium and $\sigma_{33} = \sigma_{33P_T} + \sigma_{33S_T}$ in the transmission medium. Denoting by F the vertical component of the energy flux (equation (6.147)), we obtain

$$F_{P_I} + F_{P_R} + F_{S_R} + F_{P_IP_R} + F_{P_IS_R} + F_{P_RS_R} = F_{P_T} + F_{S_T} + F_{P_TS_T}, \tag{6.148}$$

where

$$\begin{aligned}
-2F_{P_I} &= \mathrm{Re}(\sigma_{13P_I}v_{1P_I}^* + \sigma_{33P_I}v_{3P_I}^*)\\
-2F_{P_R} &= \mathrm{Re}(\sigma_{13P_R}v_{1P_R}^* + \sigma_{33P_R}v_{3P_R}^*)\\
-2F_{S_R} &= \mathrm{Re}(\sigma_{13S_R}v_{1S_R}^* + \sigma_{33S_R}v_{3S_R}^*)\\
-2F_{P_IP_R} &= \mathrm{Re}(\sigma_{13P_I}v_{1P_R}^* + \sigma_{13P_R}v_{1P_I}^* + \sigma_{33P_I}v_{3P_R}^* + \sigma_{33P_R}v_{3P_I}^*)\\
-2F_{P_IS_R} &= \mathrm{Re}(\sigma_{13P_I}v_{1S_R}^* + \sigma_{13S_R}v_{1P_I}^* + \sigma_{33P_I}v_{3S_R}^* + \sigma_{33S_R}v_{3P_I}^*)\\
-2F_{P_RS_R} &= \mathrm{Re}(\sigma_{13P_R}v_{1S_R}^* + \sigma_{13S_R}v_{1P_R}^* + \sigma_{33P_R}v_{3S_R}^* + \sigma_{33S_R}v_{3P_R}^*)\\
-2F_{P_T} &= \mathrm{Re}(\sigma_{13P_T}v_{1P_T}^* + \sigma_{33P_T}v_{3P_T}^*)\\
-2F_{S_T} &= \mathrm{Re}(\sigma_{13S_T}v_{1S_T}^* + \sigma_{33S_T}v_{3S_T}^*)\\
-2F_{P_TS_T} &= \mathrm{Re}(\sigma_{13P_T}v_{1S_T}^* + \sigma_{13S_T}v_{1P_T}^* + \sigma_{33P_T}v_{3S_T}^* + \sigma_{33S_T}v_{3P_T}^*).
\end{aligned} \tag{6.149}$$

For instance, F_{P_I} is the energy flux of the incident qP wave and $F_{P_IP_R}$ is the interference flux between the incident and reflected qP waves. In the elastic limit, it can be shown that the interference fluxes vanish. Further algebra implies that the fluxes given in the preceding equations are proportional to the real parts of

$$\begin{aligned}
F_{P_I} &\propto \beta_{P_1}^* W_{P_1} + \xi_{P_1}^* Z_{P_1}\\
F_{P_R} &\propto -(\beta_{P_1}^* W_{P_1} + \xi_{P_1}^* Z_{P_1})|R_{\mathrm{PP}}|^2\\
F_{S_R} &\propto -(\beta_{S_1}^* W_{S_1} + \xi_{S_1}^* Z_{S_1})|R_{\mathrm{PS}}|^2\\
F_{P_IP_R} &\propto -2\mathrm{i}(\beta_{P_1}^* W_{P_1} - \xi_{P_1}^* Z_{P_1})\mathrm{Im}(R_{\mathrm{PP}})\\
F_{P_IS_R} &\propto (\beta_{S_1}^* W_{P_1} - \xi_{S_1}^* Z_{P_1})R_{\mathrm{PS}}^* - (\beta_{P_1}^* W_{S_1} - \xi_{P_1}^* Z_{S_1})R_{\mathrm{PS}}\\
F_{P_RS_R} &\propto -[(\beta_{S_1}^* W_{P_1} + \xi_{S_1}^* Z_{P_1})R_{\mathrm{PP}}R_{\mathrm{PS}}^* + (\beta_{P_1}^* W_{S_1} + \xi_{P_1}^* Z_{S_1})R_{\mathrm{PP}}^* R_{\mathrm{PS}}]\\
F_{P_T} &\propto (\beta_{P_2}^* W_{P_2} + \xi_{P_2}^* Z_{P_2})|T_{\mathrm{PP}}|^2\\
F_{S_T} &\propto (\beta_{S_2}^* W_{S_2} + \xi_{S_2}^* Z_{S_2})|T_{\mathrm{PS}}|^2\\
F_{P_TS_T} &\propto (\beta_{S_2}^* W_{P_2} + \xi_{S_2}^* Z_{P_2})T_{\mathrm{PP}}T_{\mathrm{PS}}^* + (\beta_{P_2}^* W_{S_2} + \xi_{P_2}^* Z_{S_2})T_{\mathrm{PP}}^* T_{\mathrm{PS}},
\end{aligned} \tag{6.150}$$

where the proportionality factor is $\frac{1}{2}\omega^2$.

We define the energy reflection and transmission coefficients as

$$ER_{\mathrm{PP}} = \sqrt{\frac{F_{P_R}}{F_{P_I}}}, \quad ER_{\mathrm{PS}} = \sqrt{\frac{F_{S_R}}{F_{P_I}}},$$

$$ET_{\mathrm{PP}} = \sqrt{\frac{F_{P_T}}{F_{P_I}}}, \quad ET_{\mathrm{PS}} = \sqrt{\frac{F_{S_T}}{F_{P_I}}}, \tag{6.151}$$

and the interference coefficients as

$$I_{P_I P_R} = \frac{F_{P_I P_R}}{F_{P_I}}, \quad I_{P_I S_R} = \frac{F_{P_I S_R}}{F_{P_I}}, \quad I_{P_R S_R} = \frac{F_{P_R S_R}}{F_{P_I}}, \quad I_{P_T S_T} = \frac{F_{P_T S_T}}{F_{P_I}}, \tag{6.152}$$

to obtain the following energy-balance equation:

$$1 + ER^2_{\mathrm{PP}} + ER^2_{\mathrm{PS}} + I_{P_I P_R} + I_{P_I S_R} + I_{P_R S_R} = ET^2_{\mathrm{PP}} + ET^2_{\mathrm{PS}} + I_{P_T S_T}. \tag{6.153}$$

We have chosen the square root of the energy ratio (Gutenberg, 1944) since it is more nearly related to the response, in terms of particle velocities and displacements.

6.2.7 Umov-Poynting theorem, energy velocity and quality factor

The energy-balance equation or Umov-Poynting theorem for the propagation of time harmonic fields in anisotropic viscoelastic media is given in Section 4.3.1, equation (4.82). For inhomogeneous viscoelastic plane waves, it is

$$-2\boldsymbol{\alpha} \cdot \mathbf{p} = 2\mathrm{i}\omega[\langle V \rangle - \langle T \rangle] - \omega \langle D \rangle, \tag{6.154}$$

where $\langle V \rangle$ and $\langle T \rangle$ are the time-averaged strain- and kinetic-energy densities, respectively, and $\langle D \rangle = \langle \dot{D} \rangle / \omega$ is the time-averaged dissipated-energy density.

The energy velocity $\mathbf{v}_e$ is defined as the ratio of the average power-flow density $\langle \mathbf{p} \rangle$ to the mean energy density $\langle E \rangle = \langle V + T \rangle$ (equation (4.76)). Fortunately, it is not necessary to calculate the strain and kinetic energies explicitly, since, using equation (4.73) and $\omega \mathbf{s}_R = \boldsymbol{\kappa}$,

$$\langle E \rangle = \mathbf{s}_R \cdot \langle \mathbf{p} \rangle. \tag{6.155}$$

Then, the energy velocity can be calculated as

$$\mathbf{v}_e = \frac{\langle \mathbf{p} \rangle}{\mathbf{s}_R \cdot \langle \mathbf{p} \rangle}. \tag{6.156}$$

Using equations (6.110) and (6.120), we find that the energy velocity is

$$\mathbf{v}_e = \frac{\mathrm{Re}(\beta^* X + \xi^* W)\hat{\mathbf{e}}_1 + \mathrm{Re}(\beta^* W + \xi^* Z)\hat{\mathbf{e}}_3}{\mathrm{Re}(s_1)\mathrm{Re}(\beta^* X + \xi^* W) + \mathrm{Re}(s_3)\mathrm{Re}(\beta^* W + \xi^* Z)}, \tag{6.157}$$

which, by (6.142) becomes

$$\mathbf{v}_e = [\mathrm{Re}(s_1 + s_3 \cot\psi)]^{-1}\hat{\mathbf{e}}_1 + [\mathrm{Re}(s_1 \tan\psi + s_3)]^{-1}\hat{\mathbf{e}}_3. \tag{6.158}$$

An alternative expression for the energy velocity is obtained from the fact that, as in the elastic case, the phase velocity is the projection of the energy velocity onto the propagation direction (equation (4.78)). Thus, we have

$$v_e = v_p / \cos(\psi - \theta). \tag{6.159}$$

In terms of the tangents defined in equations (6.141) and (6.142), the magnitude of the energy velocity is

$$v_e = \left[\frac{\sqrt{(1+\tan^2\psi)(1+\tan^2\theta)}}{(1+\tan\psi\tan\theta)}\right] v_p. \tag{6.160}$$

The quality factor, as defined in equation (4.84), is twice the ratio of the average strain-energy density and the average dissipated-energy density, and is written as

$$Q = \frac{2\langle V\rangle}{\langle D\rangle}. \tag{6.161}$$

From equation (4.92), the quality factor of the incident homogeneous wave is simply

$$Q_{P_I} = \frac{\mathrm{Re}(v_{c1}^2)}{\mathrm{Im}(v_{c1}^2)}. \tag{6.162}$$

For the reflected and transmitted waves, we make use of the following fundamental relations derived in Section 4.3.1 (equations (4.83) and (4.71), respectively):

$$\langle D\rangle = \frac{2}{\omega}\boldsymbol{\alpha}\cdot\langle\mathbf{p}\rangle \tag{6.163}$$

and

$$\langle V\rangle = \frac{1}{2}\mathrm{Re}(\mathbf{s}^*\cdot\mathbf{p}), \tag{6.164}$$

where we have used $\omega\mathbf{s}_R = \boldsymbol{\kappa}$ and $\langle D\rangle = \langle\dot{D}\rangle/\omega$. Substitution of these relations into equation (6.161), and the use of equation (6.110) yields

$$Q = -\frac{\mathrm{Re}(\mathbf{s}^*\cdot\mathbf{p})}{2\ \mathrm{Im}(\mathbf{s})\cdot\langle\mathbf{p}\rangle}, \tag{6.165}$$

or, using equation (6.120),

$$Q = -\frac{\mathrm{Re}[(\beta^*X+\xi^*W)s_1^* + (\beta^*W+\xi^*Z)s_3^*)]}{2[\mathrm{Re}(\beta^*X+\xi^*W)\mathrm{Im}(s_1) + \mathrm{Re}(\beta^*W+\xi^*Z)\mathrm{Im}(s_3)]}. \tag{6.166}$$

Thus, we have an expression for the quality factor in terms of the complex slowness and Umov-Poynting vector, which, unlike equation (6.162), holds for inhomogeneous plane waves.

6.2.8 Reflection of seismic waves

We consider the reflection and transmission of seismic waves and compare the results with the elastic case, i.e., the case where both media are elastic. To begin, we briefly consider the following two special cases and the implications of the theory. Firstly, if the incidence medium is elastic and the transmission medium anelastic, the theory imposes that the attenuation vectors of the transmitted waves are perpendicular to the interface. Secondly, if the incidence medium is anelastic, the incident wave is homogeneous, and the transmission medium is elastic, then the transmitted waves are inhomogeneous of the elastic type, i.e., the angle between the Umov-Poynting vector and the attenuation vector

is $\pi/2$ (Theorem 2 of Section 6.1.4 considers the cross-plane wave case). The interpretation for the isotropic case is given by Krebes and Slawinski (1991).

The elastic or unrelaxed stiffnesses of the incidence medium are given by

$$c_{11} = \rho c_P^2(\pi/2), \quad c_{33} = \rho c_P^2(0), \quad c_{55} = \rho c_S^2, \quad c_{13} = 3.906 \text{ GPa},$$

where

$$c_P(\pi/2) = 2.79 \text{ km/s}, \quad c_P(0) = 2.24 \text{ km/s}, \quad c_S = 1.01 \text{ km/s}, \quad \rho = 2700 \text{ kg/m}^3.$$

It is assumed that the medium has two relaxation peaks centered at $f_0 = 12.625$ Hz ($\tau_0 = 1/2\pi f_0$), with minimum quality factors of $Q_{01} = 20$ and $Q_{02} = 15$, corresponding to dilatation and shear deformations, respectively.

On the other hand, the unrelaxed properties of the transmission medium are

$$c'_{11} = \rho' {c'_P}^2(\pi/2), \quad c'_{33} = \rho' {c'_P}^2(0), \quad c'_{55} = \rho' {c'_S}^2, \quad c'_{13} = 28.72 \text{ GPa},$$

where

$$c'_P(\pi/2) = 4.6 \text{ km/s}, \quad c'_P(0) = 4.1 \text{ km/s}, \quad c'_S = 2.4 \text{ km/s}, \quad \rho' = 3200 \text{ kg/m}^3.$$

As before, there are two relaxation peaks centered at the same frequency, with $Q_{01} = 60$ and $Q_{02} = 35$.

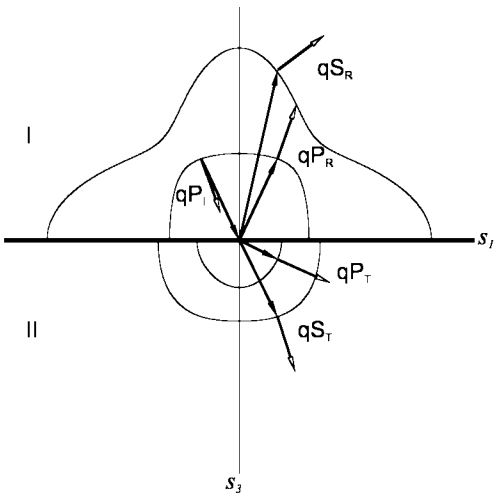

Figure 6.11: Reflected (qP_R and qS_R) and transmitted (qP_T and qS_T) plane waves for an incident qP wave with $\theta_{P_I} = 25°$. The slowness curves for homogeneous waves of the upper and lower medium are represented, with the inner curves corresponding to the quasi-compressional waves. The lines coincide with the propagation direction and the convention for the attenuation and energy vectors is that indicated in Figure 6.1.

The slowness curves for homogeneous waves are represented in Figure 6.11, where the inner curve corresponds to the qP wave. The figure also shows the attributes of the

incident, reflected and transmitted waves for an incidence angle $\theta_{P_I} = 25°$. In the anelastic case, the Umov-Poynting vectors (empty arrows) of the incident and reflected qP waves are almost perpendicular to the slowness surface. The perpendicularity property is only verified in the elastic case. The transmitted waves show a high degree of inhomogeneity – i.e., the propagation and attenuation vectors do not have the same direction. This is true, in particular, for the qP wave, whose attenuation vector is almost perpendicular to the direction of the energy vector.

Figure 6.12 represents the absolute value of the amplitude coefficients versus the incidence propagation angle for the elastic (a) and viscoelastic (b) cases. If the two media are elastic, there is a critical angle at approximately 27°, which occurs when the Umov-Poynting vector of the transmitted qP wave becomes parallel to the interface. If the lower medium is anelastic or both media are anelastic, the energy vector of the transmitted qP wave points downwards for all the incidence propagation angles. Thus, there is no critical angle. This can be seen in Figure 6.13, where the absolute values of the energy coefficients are displayed as a function of θ_{P_I} (a) and ψ_{P_I} (b). Since ET_{PP} is always strictly greater than zero, the P_T Umov-Poynting vector is never parallel to the interface.

The propagation, energy and attenuation angles, as a function of the incidence angle, are represented in Figure 6.14. By symmetry, the propagation and energy angles of the reflected P_R wave are equal to θ_{P_I} and ψ_{P_I}, respectively. For viscoelastic plane waves traveling in an anisotropic medium, $|\theta - \delta|$ may exceed 90°. However, the difference $|\psi - \delta|$ must be less than 90°. Indeed, since the energy loss is always positive, equation (6.163) implies that the magnitude of the angle between $\boldsymbol{\alpha}$ and $\langle \mathbf{p} \rangle$ is always strictly less than $\pi/2$. This property is verified in Figure 6.14. Moreover, this figure shows that, at approximately the elastic critical angle and beyond, the P_T energy angle is close to $\pi/2$ and that the attenuation vector is almost perpendicular to the interface. This indicates that, practically, the transmitted qP wave behaves as an evanescent wave of the elastic type beyond the (elastic) critical angle.

Figure 6.15 displays the phase shifts versus incidence propagation angle, indicating that there are substantial differences between the elastic (a) and the anelastic (b) cases. The phase velocities are represented in Figure 6.16. They depend on the propagation direction, mostly because the media are anisotropic, but, to a lesser extent, also because of their viscoelastic inhomogeneous character. Despite the fact that there is no critical angle, the phase velocity of the transmitted qP wave shows a similar behavior – in qualitative terms – to the elastic phase velocity. Beyond the elastic critical angle, the velocity is mainly governed by the value of the horizontal slowness, and finally approaches the phase velocity of the incidence wave. The attenuation curves (see Figure 6.17) show that dissipation of the S_R and P_T waves is very anisotropic. In particular the P_T attenuation is very high after the elastic critical angle, due to the evanescent character of the wave.

Figure 6.18 shows the energy velocity of the different waves. The difference between energy and phase velocities is due solely to the anisotropy, since they coincide in isotropic media. The quality factors are represented in Figure 6.19. Below the critical angle, the higher quality factor is that of the P_T wave, in agreement with its attenuation curve displayed in Figure 6.17. However, beyond that angle, the quality factor seems to contradict the attenuation curve of the other waves: the very strong attenuation is not reflected in the quality factor. This apparent paradox means that the usual relation $\boldsymbol{\alpha} \approx \omega \mathbf{s}_R/2Q$ (equation (4.94)) is not valid for evanescent-type waves traveling closer to interfaces, even

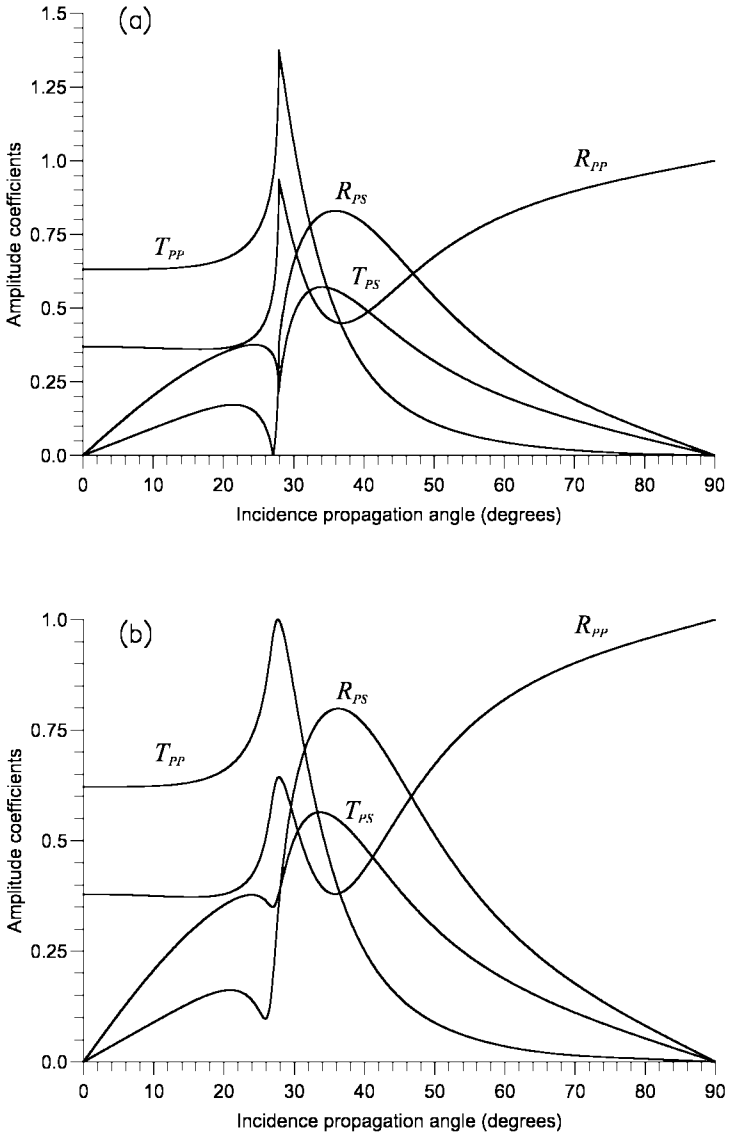

Figure 6.12: Absolute values of the reflection and transmission amplitude coefficients versus incidence propagation angle corresponding to the elastic (a) and viscoelastic (b) cases.

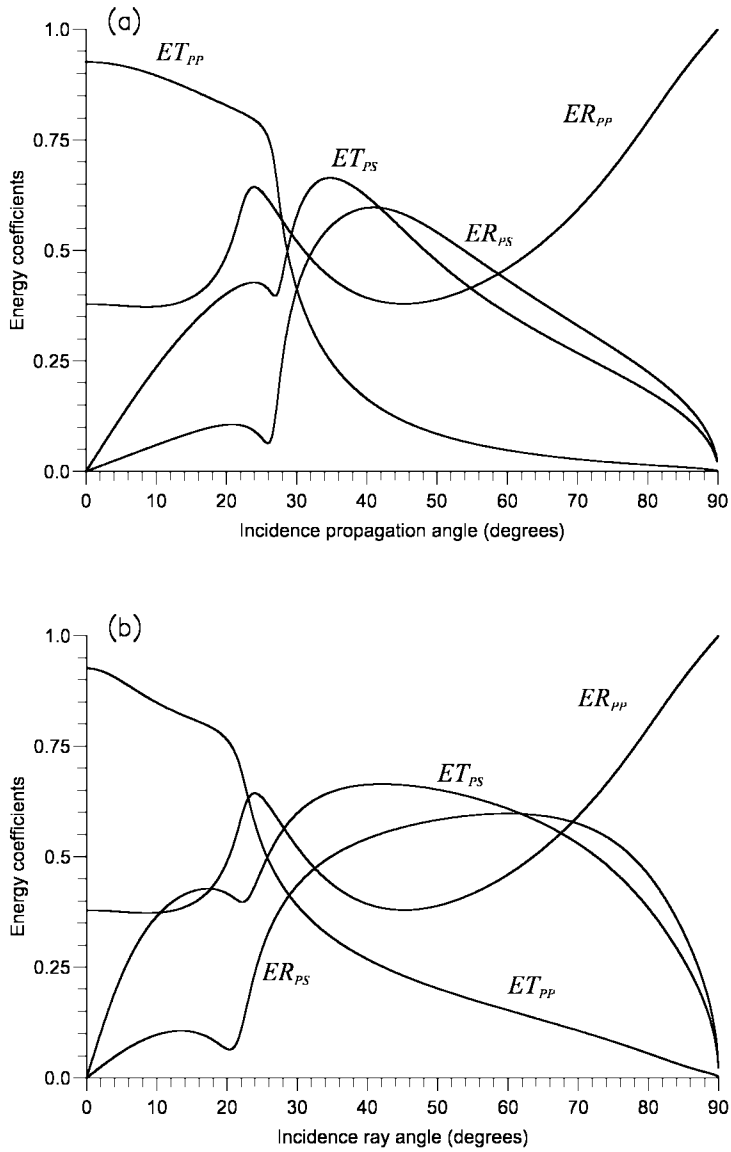

Figure 6.13: Absolute values of the reflection and transmission energy coefficients versus incidence propagation angle (a) and ray (energy) angle (b) corresponding to the viscoelastic case.

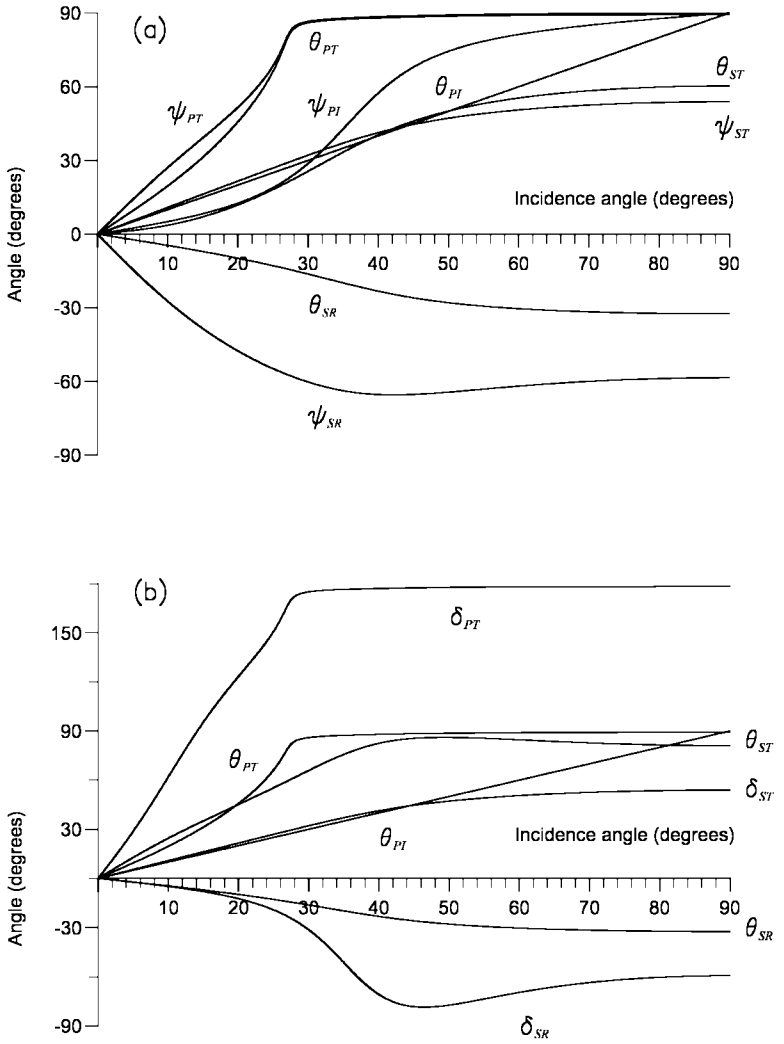

Figure 6.14: Energy (a) and attenuation (b) angles versus incidence angle for the incident, reflected and transmitted waves. The propagation angle is also represented in both cases.

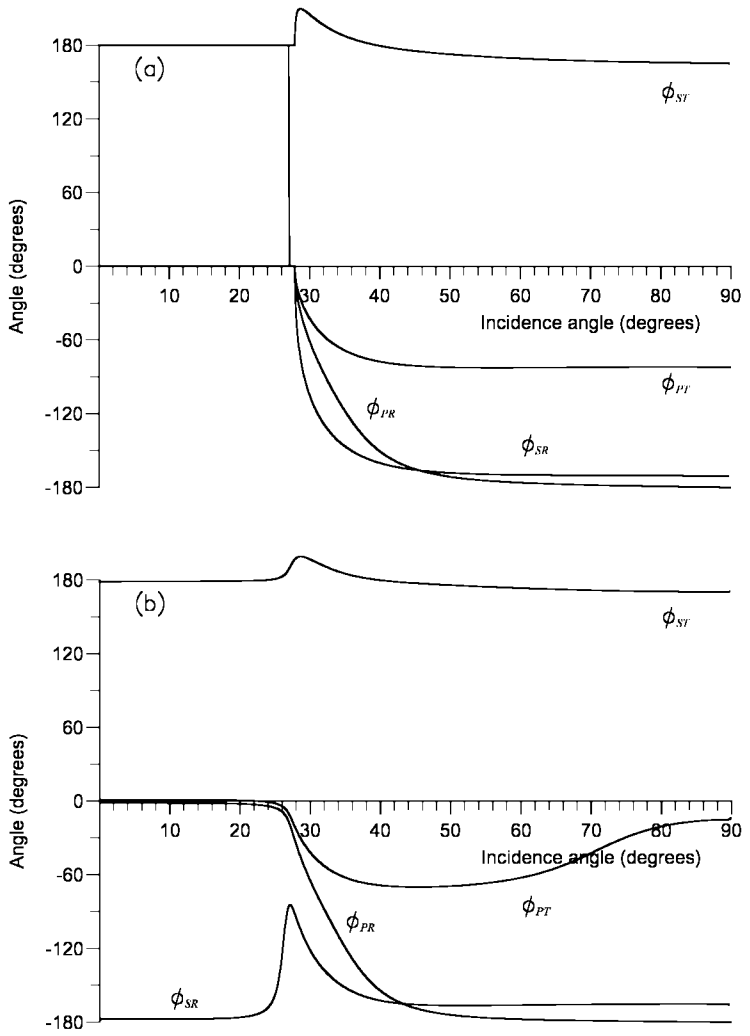

Figure 6.15: Phase angles versus incidence propagation angle for the incident, reflected and transmitted waves corresponding to the elastic (a) and viscoelastic (b) cases.

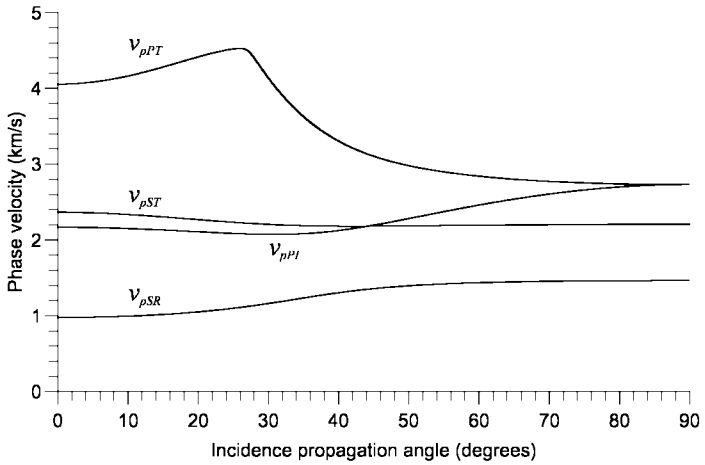

Figure 6.16: Phase velocities of the incident, reflected and transmitted waves versus the incidence propagation angle for the viscoelastic case.

if $Q \gg 1$. Finally, Figure 6.20 shows the square root of the interference coefficients versus the incidence propagation angle. It indicates that much of the energy is lost due to interference between the different waves beyond the elastic critical angle. The interference between the P_T and S_T waves is particularly high and is comparable to ET_{PP} around 30° incidence. Note that these coefficients vanish in the elastic case.

The reflection-transmission problem can be solved for transient fields by using the equations given in Section 4.5.4. A wave modeling algorithm based on the Fourier pseudospectral method is used to compute the spatial derivatives, and a fourth-order Runge-Kutta technique to compute the wave field recursively in time (see Chapter 9). The numerical mesh has 231 × 231 points with a grid spacing of 20 m. The source is a Ricker-type wavelet located at 600 m above the interface, and has a dominant frequency of 12.625 Hz, i.e., the central frequency of the relaxation peaks. In order to generate mainly qP energy, the source is a discrete delta function, equally distributed in the stress components σ_{11} and σ_{33} – a mean stress perturbation. Figure 6.21 shows a snapshot at 800 ms, which covers the incidence ray angles from 0° to approximately 62°. In the upper medium, the primary waves are the qP wave followed by the qS wave, which shows high amplitude cuspidal triangles despite the dilatational nature of the source. Moreover, the P_R and S_R are traveling upwards, away from the interface. Near the center of the mesh, the events are mainly related to the reflection of the cuspidal triangles. In the lower medium, the P_T wave is followed by the S_T wave, which resembles a continuation of the incident qP wave, since both events have similar velocities (see Figure 6.11). In principle, Figure 6.21 should be interpreted by comparison with Figure 6.13. However, Figure 6.21 displays the vertical particle velocity v_3, and Figure 6.13b the square root of the normal power flow. Moreover, the interpretation must take into account that the source has a non-isotropic radiation pattern, and that the incidence wave is also affected by anisotropic attenuation effects. Despite these considerations, a qualitative interpretation can be attempted. First,

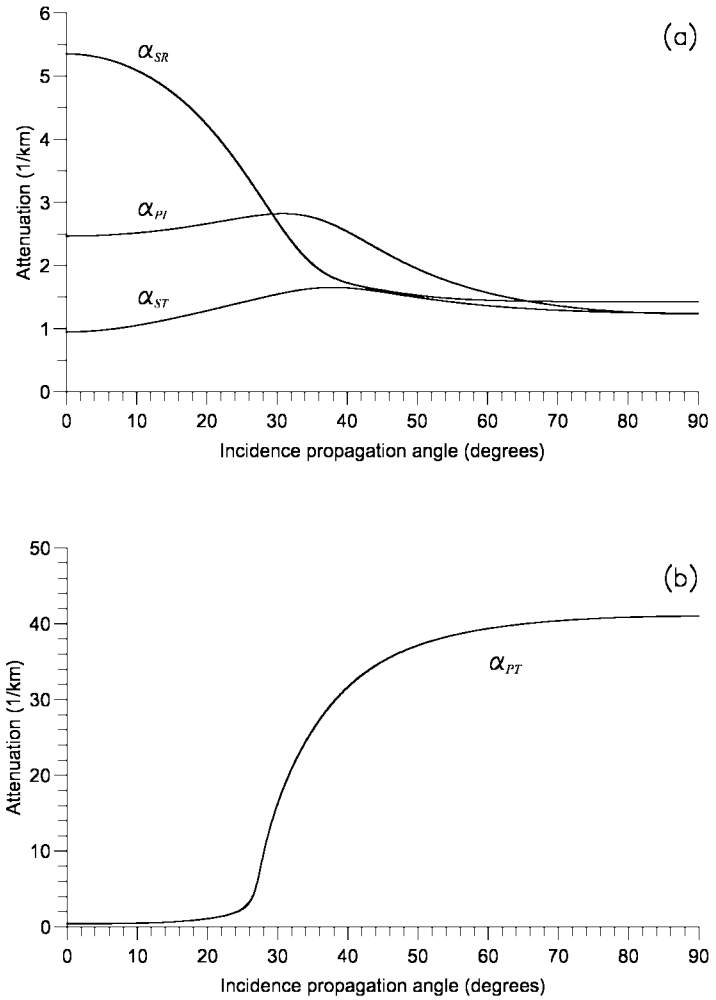

Figure 6.17: Attenuations of the incident, reflected and transmitted waves versus the incidence propagation angle. Figure 6.17b corresponds to the transmitted quasi-compressional wave.

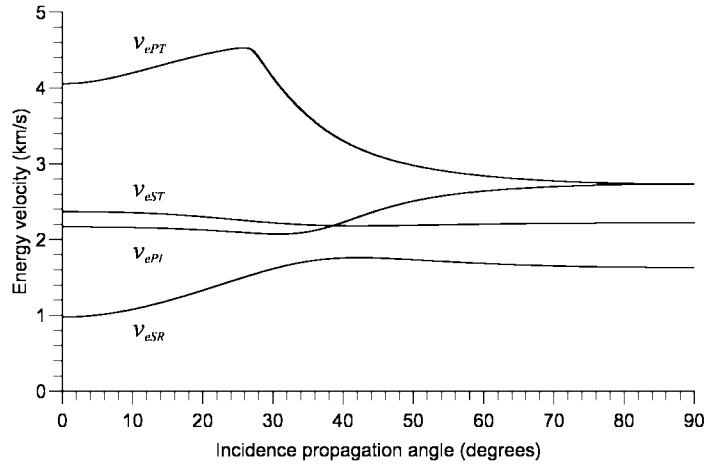

Figure 6.18: Energy velocities of the incident, reflected and transmitted waves versus the incidence propagation angle for the viscoelastic case.

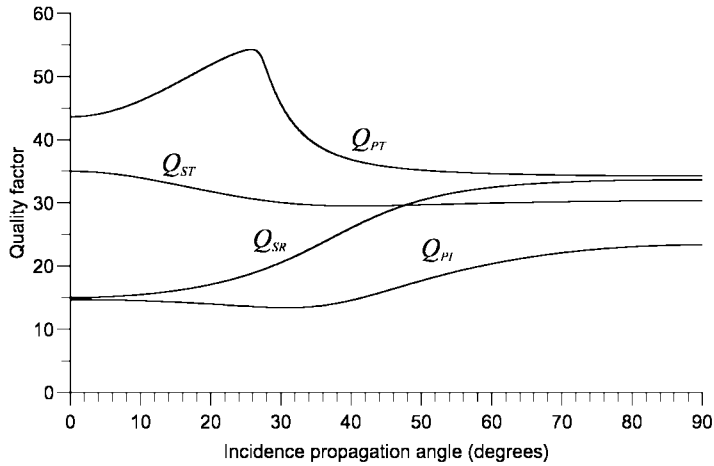

Figure 6.19: Quality factors of the incident, reflected and transmitted waves versus the incidence propagation angle for the viscoelastic case.

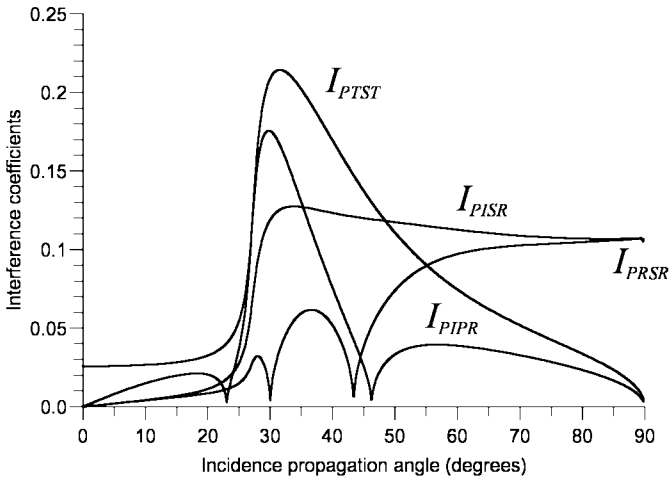

Figure 6.20: Square root of the interference coefficients versus the incidence propagation angle.

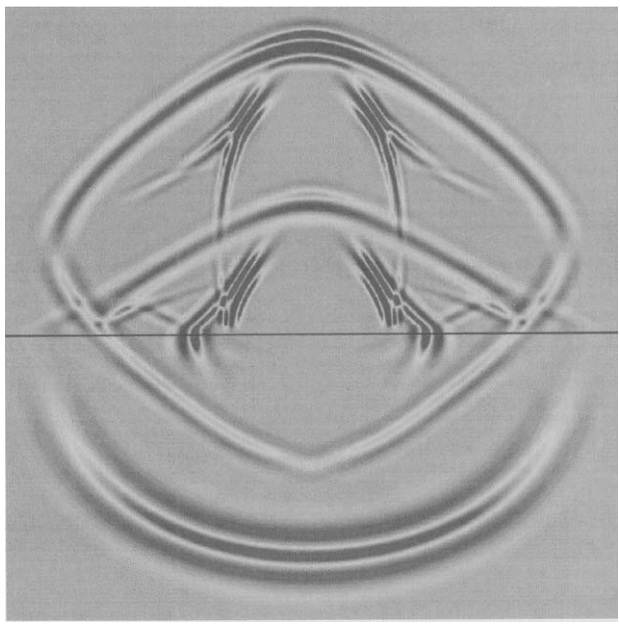

Figure 6.21: Snapshot of the vertical particle-velocity component v_3, corresponding to the viscoelastic reflection-transmission problem at 800 ms.

the amplitudes of the S_R and S_T waves are very low at normal incidence, as predicted by the ER_{PS} and ET_{PS} curves, respectively. In particular, the amplitude of the S_T wave increases for increasing ray angle, in agreement with ET_{PS}. In good agreement also, is the amplitude variation of the P_T wave compared to the ET_{PP} curve. Another event is the planar wave front connecting the reflected and transmitted qP waves. This is a conical or head wave that cannot be entirely explained by the plane-wave analysis. Despite the fact that a critical angle does not exist, since ψ_{PT} never reaches $\pi/2$ (see Figure 6.14a), some of the P_T energy disturbs the interface, giving rise to the conical wave.

6.2.9 Incident inhomogeneous waves

In the previous section, we assumed incident homogeneous waves. Here, we consider the more realistic case of inhomogeneous plane waves, illustrated with a geophysical example. In offshore seismic exploration, the waves transmitted at the ocean bottom have a particular characteristic. Assuming that water is lossless and using Snell's law (Section 3.5), their attenuation vectors are perpendicular to the ocean-bottom interface. This fact affects the amplitude variations with offset (AVO) of reflection events generated at the lower layers.

Winterstein (1987) investigates the problem from a "kinematic" point of view. He analyzes how the angle between propagation and maximum attenuation varies in an anelastic layered medium, and shows that departures from elastic wave ray paths can be large. In addition, compressional-wave reflection coefficients for different incidence inhomogeneity angles are compared by Krebes (1984). He shows that the deviations from the elastic case can be important at supercritical angles.

Here, we study the AVO response for an inhomogeneous wave generated at the ocean bottom and incident at a lower interface separating two viscoelastic transversely isotropic media. Unlike the analysis performed by Krebes (1984), the inhomogeneity angle is not constant with offset, but is equal to the incidence angle, since the interface is assumed to be parallel to the ocean bottom (see Figure 6.22). The interface may separate two finely layered formations whose contact plane is parallel to the stratification, or two media with intrinsic anisotropic properties, such as shale and limestone.

The consistent 2-D stress-strain relation for qP-qS propagation is given in Section 4.5.4, based on model 3 (see Section 4.1.3). The convention is to denote the quasi-dilatational and quasi-shear deformations with $\nu = 1$ and $\nu = 2$, respectively. The complex stiffnesses relating stress and strain for a 2-D transversely isotropic medium (4.161) can be expressed as

$$\begin{aligned}
p_{11} &= c_{11} - \tfrac{1}{2}(c_{11}+c_{33}) + \left[\tfrac{1}{2}(c_{11}+c_{33}) - c_{55}\right] M_1 + c_{55} M_2 \\
p_{33} &= c_{33} - \tfrac{1}{2}(c_{11}+c_{33}) + \left[\tfrac{1}{2}(c_{11}+c_{33}) - c_{55}\right] M_1 + c_{55} M_2 \\
p_{13} &= c_{13} - \tfrac{1}{2}(c_{11}+c_{33}) + \left[\tfrac{1}{2}(c_{11}+c_{33}) - c_{55}\right] M_1 + c_{55}(2 - M_2) \\
p_{55} &= c_{55} M_2.
\end{aligned} \tag{6.167}$$

The elasticity constants c_{IJ}, $I, J = 1, \ldots, 6$ are the unrelaxed or high-frequency limit stiffnesses, and $M_\nu(\omega)$ are dimensionless complex moduli. For one Zener mechanism, M_ν is given in equation (4.6). The form of $M_\nu(\omega)$ for L Zener models connected in parallel is given in equation (2.196). In the lossless case ($\omega \to \infty$), $M_\nu \to 1$.

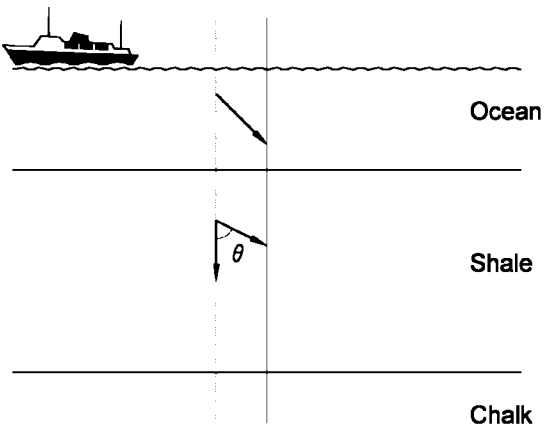

Figure 6.22: Snell's law for a plane wave incident on the ocean-bottom interface. The diagram shows the continuity of the horizontal component of the complex-slowness vector. In the ocean, this vector is real, since water is assumed to be lossless. In the shale layer the attenuation vector is perpendicular to the ocean bottom.

Generation of inhomogeneous waves

Let us assume that the positive z-axis points downwards. A general solution for the particle-velocity field $\mathbf{v} = (v_1, v_3)$ is

$$\mathbf{v} = \mathrm{i}\omega\mathbf{U}\exp\left[\mathrm{i}\omega(t - s_1 x - s_3 z)\right], \tag{6.168}$$

where s_1 and s_3 are the components of the complex-slowness vector and $\mathbf{U}$ is a complex vector. The slowness vector

$$\mathbf{s}_R = (\mathrm{Re}(s_1), \mathrm{Re}(s_3)) \tag{6.169}$$

and the attenuation vector

$$\boldsymbol{\alpha} = -\omega(\mathrm{Im}(s_1), \mathrm{Im}(s_3)), \tag{6.170}$$

in general, will not point in the same direction. Figure 6.22 depicts a transmitted inhomogeneous wave generated at the ocean bottom. As mentioned before, since the attenuation vector of waves propagating in the water layer is zero, the viscoelastic Snell's law implies that the attenuation vector of the transmitted wave is perpendicular to the ocean bottom. Note that the inhomogeneity angle is equal to the propagation angle θ.

The complex-slowness components below the ocean bottom are

$$s_1 = s_R \sin\theta, \quad s_3 = s_R \cos\theta - \frac{\mathrm{i}\alpha}{\omega}, \tag{6.171}$$

where s_R and α are the magnitudes of $\mathbf{s}_R$ and $\boldsymbol{\alpha}$, respectively. For a given angle θ, s_R and α can be computed from the dispersion relation (6.113). Then, the substitution of these quantities into equation (6.171) yields the slowness components of the incident inhomogeneous wave. However, this method requires the numerical solution of two fourth-degree polynomials. A simpler approach is the following:

1. Assume a given propagation angle θ_H for a hypothetical transmitted homogeneous wave below the ocean bottom. Then, according to equation (6.125), the complex slowness is
$$s = \sqrt{2\rho}\,(p_{55} + p_{11}\sin^2\theta_H + p_{33}\cos^2\theta_H \pm C)^{-1/2}, \tag{6.172}$$
where ρ is the density and C is given by equation (6.126) with $\theta = \theta_H$.

2. Choose s_1 for the inhomogeneous wave equal to $\mathrm{Re}(s)\sin\theta_H$, a real quantity – according to Snell's law – since the projection of $\boldsymbol{\alpha}$ on the interface is zero.

3. Compute s_3 from the dispersion relation (6.113).

4. Compute the incidence propagation angle θ for the inhomogeneous wave from $\sin\theta = s_1/|s|$ as
$$\theta = \arcsin\left(\frac{s_1}{\sqrt{s_1^2 + [\mathrm{Re}(s_3)]^2}}\right). \tag{6.173}$$

In this way, a vector (s_1, s_3), satisfying equation (6.113) and providing input to the reflection-transmission problem, can be obtained for each incidence angle θ. The price we pay for this simplicity is that the ray angle does not reach 90°, but this is not relevant since the offsets of interest in exploration geophysics are sufficiently covered.

Ocean bottom

The material properties of the incidence and transmission media – shale and chalk, respectively – are given in Table 6.1, where $v_{IJ} = \sqrt{c_{IJ}/\rho}$.

Table 6.1. Material properties

ROCK	v_{11} (m/s)	v_{33} (m/s)	v_{55} (m/s)	v_{13} (m/s)	Q_{01}	Q_{02}	ρ (g/cm^3)
shale	3810	3048	1402	1828	10	5	2.3
chalk	5029	5029	2621	3414	100	70	2.7

The unrelaxed velocities are indicated in the table, and attenuation is quantified by the parameters $Q_{0\nu} = \mathrm{Re}(M_\nu)/\mathrm{Im}(M_\nu)$ at the reference frequency. Wright (1987) calculates the reflection coefficients for the elastic case, which is obtained in the unrelaxed limit.

The comparison between the absolute values of the qP wave reflection coefficients, together with the corresponding phase angles, is shown in Figure 6.23. In the figure, "E" corresponds to the elastic case (i.e., elastic shale), "H" to an incident viscoelastic homogeneous wave, and "I" to an incident inhomogeneous wave with the characteristics indicated in Figure 6.22 – the chalk is assumed anelastic in the three cases. In the elastic case, i.e., shale and chalk both elastic (Wright, 1987), there is a critical angle between 40° and 50°. It can be shown that the energy vector of the transmitted qP wave points downwards for all incidence angles. Thus, there is no critical angle in the strict sense. However, the shape of the E and I curves indicates that a quasi-evanescent wave propagates through the interface. This character is lost in the H curve. In the near-offsets

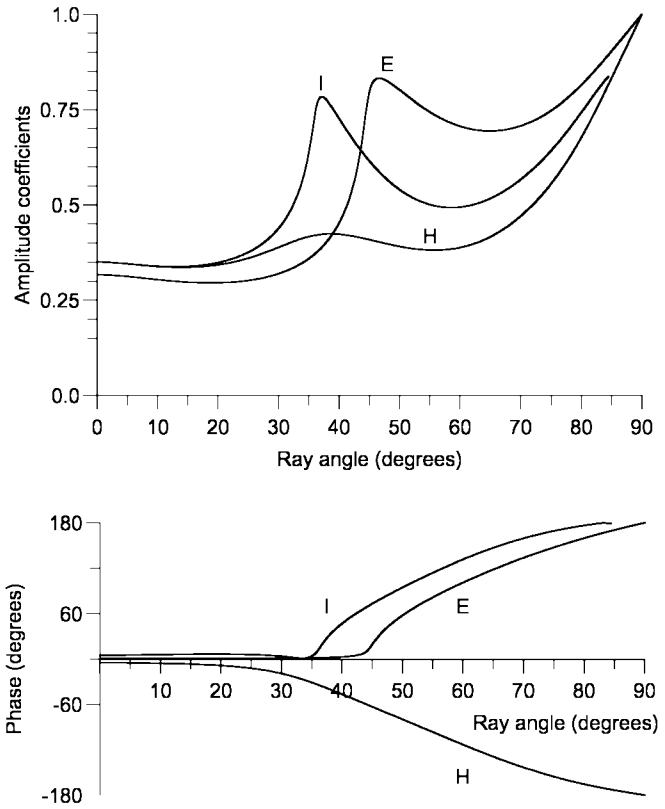

Figure 6.23: Comparison between the absolute values of the R_{PP} reflection coefficients together with the corresponding phase angles, where "E" corresponds to the elastic case (i.e., elastic shale), "H" to an incident viscoelastic homogeneous wave, and "I" to an incident inhomogeneous wave exhibiting the characteristics indicated in Figure 6.22.

– up to 20° – the three coefficients follow the same trend and are very similar to each other. The difference between this case and the elastic case (E) is due to the anelastic properties of the shale. Beyond 30°, the differences are important, mainly for the incident homogeneous wave. These can also be observed in the phase where the H curve has the opposite sign with respect to the other curves. A similar effect is reported by Krebes (1984). More details and results about this problem are given by Carcione (1999b).

6.3 Reflection and transmission at fluid/solid interfaces.

Fluid/solid interfaces are important in seismology and exploration geophysics, particularly in offshore seismic prospecting, where the ocean bottom is one of the main reflection events. We consider this problem by assuming an incident homogeneous P wave.

6.3.1 Solid/fluid interface

A general plane-wave solution for the particle-velocity field $\mathbf{v} = (v_1, v_3)$ is

$$\mathbf{v} = \mathrm{i}\omega \mathbf{U} \exp\left[\mathrm{i}\omega(t - s_1 x - s_3 z)\right], \tag{6.174}$$

where $\mathbf{U}$ is a complex vector of magnitude U. For homogeneous waves,

$$s_1 = \sin\theta / v_{P_1}, \tag{6.175}$$

where θ is the propagation angle measured with respect to the z-axis, and v_{P_1} is the complex velocity, in this case, the complex P-wave velocity of the solid. Let us denote the complex S-wave velocity of the solid by v_{S_1} and the complex P-wave velocity of the fluid by v_{P_2}.

The upper viscoelastic medium (the solid) is denoted by subscript 1 and the viscoacoustic medium (the fluid) by subscript 2. The symbol P indicates the compressional wave in the fluid or the P wave in the upper layer, and S denotes the S wave in this medium. As before, the subscripts I, R and T denote the incident, reflected and transmitted waves. Using symmetry properties to define the polarization of the reflected waves and using the fact that Snell's law implies the continuity of the horizontal slowness s_1 (see Section 3.5), we note that the particle velocities for a P wave incident from the upper medium are given by

$$\mathbf{v}_1 = \mathbf{v}_{P_I} + \mathbf{v}_{P_R} + \mathbf{v}_{S_R}, \tag{6.176}$$

$$\mathbf{v}_2 = \mathbf{v}_{P_T}, \tag{6.177}$$

where

$$\mathbf{v}_{P_I} = \mathrm{i}\omega(\beta_{P_1}, \xi_{P_1}) \exp\left[\mathrm{i}\omega(t - s_1 x - s_{3P_1} z)\right], \tag{6.178}$$

$$\mathbf{v}_{P_R} = \mathrm{i}\omega R_{\mathrm{PP}}(\beta_{P_1}, -\xi_{P_1}) \exp\left[\mathrm{i}\omega(t - s_1 x + s_{3P_1} z)\right], \tag{6.179}$$

$$\mathbf{v}_{S_R} = \mathrm{i}\omega R_{\mathrm{PS}}(\beta_{S_1}, -\xi_{S_1}) \exp\left[\mathrm{i}\omega(t - s_1 x + s_{3S_1} z)\right]. \tag{6.180}$$

$$\mathbf{v}_{P_T} = \mathrm{i}\omega T_{\mathrm{PP}}(\beta_{P_2}, \xi_{P_2}) \exp\left[\mathrm{i}\omega(t - s_1 x - s_{3P_2} z)\right], \tag{6.181}$$

and the choice $U = 1$ implies no loss of generality. If we assume an isotropic solid, the slownesses and vertical slowness components are

$$\begin{aligned} s_{P_1} &= 1/v_{P_1}, \quad s_{3P_1} = \mathrm{pv}\sqrt{s_{P_1}^2 - s_1^2} \\ s_{S_1} &= 1/v_{S_1}, \quad s_{3S_1} = \mathrm{pv}\sqrt{s_{S_1}^2 - s_1^2} \\ s_{P_2} &= 1/v_{P_2}, \quad s_{3P_2} = \mathrm{pv}\sqrt{s_{P_2}^2 - s_1^2}, \end{aligned} \tag{6.182}$$

and the polarizations are

$$\beta_{P_m} = \frac{s_1}{s_{P_m}}, \quad \xi_{P_m} = \frac{s_{3P_m}}{s_{P_m}}, \quad \beta_{S_1} = \frac{s_{3S_1}}{s_{S_1}}, \quad \xi_{S_1} = -\frac{s_1}{s_{S_1}}, \quad m = 1, 2. \tag{6.183}$$

The boundary conditions require continuity of

$$v_3, \quad \sigma_{33}, \quad \text{and} \quad \sigma_{13}(= 0). \tag{6.184}$$

These conditions generate the following matrix equation for the reflection and transmission coefficients:

$$\begin{pmatrix} \xi_{P_1} & \xi_{S_1} & \xi_{P_2} \\ Z_{P_1} & Z_{S_1} & -Z_{P_2} \\ W_{P_1} & W_{S_1} & 0 \end{pmatrix} \cdot \begin{pmatrix} R_{\mathrm{PP}} \\ R_{\mathrm{PS}} \\ T_{\mathrm{PP}} \end{pmatrix} = \begin{pmatrix} \xi_{P_1} \\ -Z_{P_1} \\ W_{P_1} \end{pmatrix}, \tag{6.185}$$

where, for P_1 or S_1

$$Z = \rho_1 v_{P_1}^2 \xi s_3 + \rho_1 (v_{P_1}^2 - 2v_{S_1}^2)\beta s_1, \quad W = \rho_1 v_{S_1}^2 (\beta s_3 + \xi s_1) \tag{6.186}$$

for the upper medium – depending on the wave type, the subindex of ξ, β and s_3 is P_1 or S_1 – and

$$Z_{P_2} = \rho_2 v_{P_2}^2 (\xi_{P_2} s_{3_{P_2}} + \beta_{P_2} s_1), \quad W_{P_2} = 0 \tag{6.187}$$

for the fluid.

6.3.2 Fluid/solid interface

In this case, the fluid is denoted by the subscript 1 and the lower layer by the subscript 2. The particle velocities for a P wave incident from the fluid are given by

$$\mathbf{v}_1 = \mathbf{v}_{P_I} + \mathbf{v}_{P_R}, \tag{6.188}$$

$$\mathbf{v}_2 = \mathbf{v}_{P_T} + \mathbf{v}_{S_T}, \tag{6.189}$$

where

$$\mathbf{v}_{P_I} = \mathrm{i}\omega(\beta_{P_1}, \xi_{P_1}) \exp\left[\mathrm{i}\omega(t - s_1 x - s_{3P_1} z)\right], \tag{6.190}$$

$$\mathbf{v}_{P_R} = \mathrm{i}\omega R_{\mathrm{PP}}(\beta_{P_1}, -\xi_{P_1}) \exp\left[\mathrm{i}\omega(t - s_1 x + s_{3P_1} z)\right], \tag{6.191}$$

$$\mathbf{v}_{P_T} = \mathrm{i}\omega T_{\mathrm{PP}}(\beta_{P_2}, \xi_{P_2}) \exp\left[\mathrm{i}\omega(t - s_1 x - s_{3P_2} z)\right], \tag{6.192}$$

$$\mathbf{v}_{S_T} = \mathrm{i}\omega T_{\mathrm{PS}}(\beta_{S_2}, \xi_{S_2}) \exp\left[\mathrm{i}\omega(t - s_1 x - s_{3S_2} z)\right]. \tag{6.193}$$

The boundary conditions (6.184) generate the following matrix equation for the reflection and transmission coefficients:

$$\begin{pmatrix} \xi_{P_1} & \xi_{P_2} & \xi_{S_2} \\ Z_{P_1} & -Z_{P_2} & -Z_{S_2} \\ 0 & W_{P_2} & W_{S_2} \end{pmatrix} \cdot \begin{pmatrix} R_{\mathrm{PP}} \\ T_{\mathrm{PP}} \\ T_{\mathrm{PS}} \end{pmatrix} = \begin{pmatrix} \xi_{P_1} \\ -Z_{P_1} \\ 0 \end{pmatrix}, \tag{6.194}$$

where β_{P_1}, β_{P_2}, β_{S_2}, ξ_{P_1}, ξ_{P_2}, ξ_{S_2}, Z_{P_1}, Z_{P_2}, Z_{S_2}, W_{P_2} and W_{S_2} are obtained from equations (6.183), (6.186) and (6.187), with the material indices interchanged.

The reflection and transmission equations for an anisotropic viscoelastic solid are similar to equations (6.185) and (6.194), but use the appropriate expressions for the β's, ξ's, Z's and the W's. (This exercise is left to the reader.)

6.3.3 The Rayleigh window

In this section, we use the reflection-transmission theory to explain a phenomenon that cannot be modeled with a lossless stress-strain relation. Brekhovskikh (1960, p. 34) observed that the amplitude reflection coefficient measured for a water-steel interface was not consistent with that predicted by the elastic theory. Beyond the elastic S critical angle, there is reduction in amplitude of the reflected P wave in a narrow window. Because this occurs for an angle where the apparent phase velocity of the incident wave is near that of the Rayleigh surface wave, the phenomenon is called the "Rayleigh window". The corresponding reflection coefficient was measured experimentally by F. Becker and R. Richardson, and their ultrasonic experiments were verified with an anelastic model in a later paper (Becker and Richardson, 1972). Borcherdt, Glassmoyer and Wennerberg (1986) compared theoretical and experimental results corresponding to the same experiment, and show that the same phenomenon takes place at ocean-bottom interfaces. They find that the anelastic Rayleigh window should be observable in appropriate sets of wide-angle reflection data and can be useful in estimating attenuation for various ocean-bottom reflectors. The presence of inhomogeneous viscoelastic waves accounts for the existence of the anelastic Rayleigh window.

The scattering equations involved in this problem are given in Section 6.3.2. The complex velocity of the fluid – a viscoacoustic medium – is

$$v_{P_1} = c_{P_1}\sqrt{M}, \qquad M(\omega) = \frac{\sqrt{Q_0^2+1} - 1 + \mathrm{i}\omega Q_0 \tau_0}{\sqrt{Q_0^2+1} + 1 + \mathrm{i}\omega Q_0 \tau_0}, \tag{6.195}$$

where c_{P_1} is the unrelaxed wave velocity of water, and M is a dimensionless complex modulus. At $\omega_0 = 1/\tau_0$, the quality factor of water has the lowest value Q_0 (see Section 4.1 and equation (4.6)).

The complex Lamé constants for steel are given by

$$\mathcal{E}_2 = \rho_2 \left[\left(c_{P_2}^2 - \frac{4}{3} c_{S_2}^2 \right) M_1 + \frac{4}{3} c_{S_2}^2 M_2 \right] \quad \text{and} \quad \mu_2 = \rho_2 c_{S_2}^2 M_2, \tag{6.196}$$

where c_{P_2} and c_{S_2} are the unrelaxed P- and S-wave velocities of steel, and M_1 and M_2 are dimensionless complex moduli, defined in equation (4.6).

The properties of water are $c_{P_1} = 1490$ m/s, $\rho_1 = 1000$ kg/m^3, and $Q_0^{-1} = 0.00012$ at $f_0 = 10$ MHz ($f_0 = 1/2\pi\tau_0$). The unrelaxed velocities of steel are $c_{P_2} = 5761$ m/s, and c_{S_2}

$= 3162$ m/s, respectively, the density is $\rho_2 = 7932$ kg/m^3 and the dissipation factors at 10 MHz are $Q_{01}^{-1} = 0.0037$ and $Q_{02}^{-1} = 0.0127$. We recall that Q_{01} is a quality factor associated with dilatational deformations and not with the compressional wave. These properties give the homogeneous P- and S-wave dissipation factors and phase velocities indicated in Table 1 of Borcherdt, Glassmoyer and Wennerberg (1986), for a frequency of 10 MHz. Figure 6.24 represents the reflection coefficient (solid line), compared to the experimental values (open circles). The dashed line corresponds to the elastic case. This experiment and its theoretical prediction is a demonstration of the existence of inhomogeneous body waves.

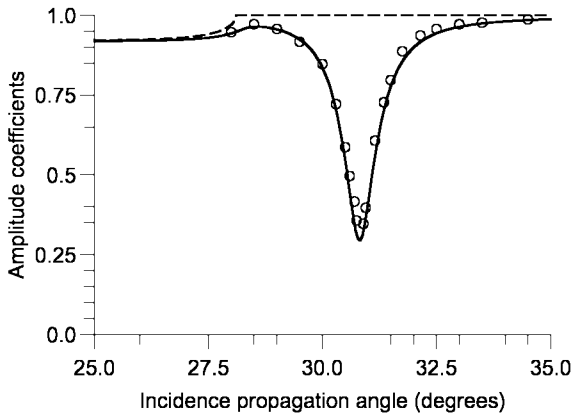

Figure 6.24: Amplitude reflection coefficient predicted for the anelastic Rayleigh window by a viscoelastic model (solid line), compared to the experimental values (open circles) (Becker and Richardson, 1972) for a water-stainless steel interface. The dashed line corresponds to the elastic case.

6.4 Reflection and transmission coefficients of a set of layers

The propagation of waves in solid layers has numerous applications in acoustics and optics. In seismology, for instance, a plane layered system can be a good representation of a stratified Earth. Let a plane wave, with horizontal complex slowness s_1, be incident on the symmetry plane of an orthorhombic medium, as shown in Figure 6.25. Inside the layer, the particle-velocity field is a superposition of upgoing and downgoing quasi-compressional (P) and quasi-shear waves (S) of the form

$$\mathbf{v} = \begin{pmatrix} v_1 \\ v_3 \end{pmatrix} = \mathrm{i}\omega \left[U_P^- \begin{pmatrix} \beta_P \\ -\xi_P \end{pmatrix} \exp(\mathrm{i}\omega s_{3P} z) + U_S^- \begin{pmatrix} \beta_S \\ -\xi_S \end{pmatrix} \exp(\mathrm{i}\omega s_{3S} z) \right.$$

$$\left. + U_P^+ \begin{pmatrix} \beta_P \\ \xi_P \end{pmatrix} \exp(-\mathrm{i}\omega s_{3P} z) + U_S^+ \begin{pmatrix} \beta_S \\ \xi_S \end{pmatrix} \exp(-\mathrm{i}\omega s_{3S} z) \right] \exp[\mathrm{i}\omega(t - s_1 x)], \qquad (6.197)$$

where U^- are upgoing-wave amplitudes, U^+ are downgoing-wave amplitudes, and β and ξ are the polarization components, given in equations (6.116) and (6.117), respectively. The vertical slowness components s_{3P} and s_{3S} are given in equation (6.114). Normal stresses and strains are related by

$$\mathrm{i}\omega\sigma_{33} = p_{13}\partial_1 v_1 + p_{33}\partial_3 v_3, \tag{6.198}$$

$$\mathrm{i}\omega\sigma_{13} = p_{55}(\partial_3 v_1 + \partial_1 v_3) \tag{6.199}$$

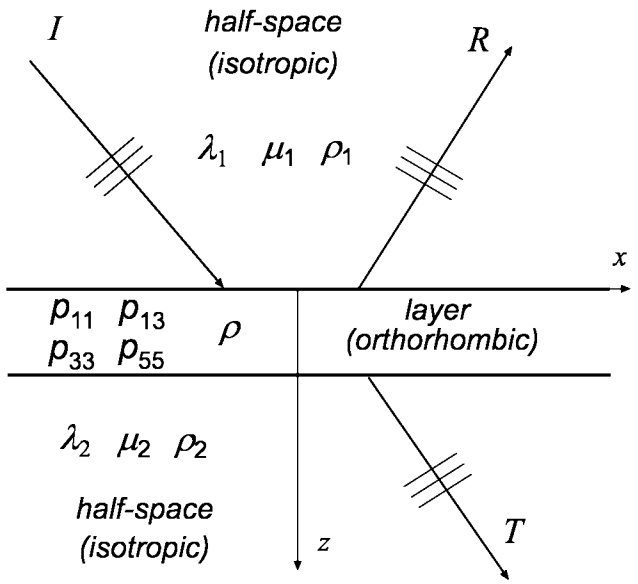

Figure 6.25: Diagram showing an orthorhombic layer embedded between two isotropic half-spaces.

Using equations (6.197), (6.198) and (6.199), the particle-velocity/stress array, inside the layer at depth z, can be written as

$$\mathbf{t}(z) = \begin{pmatrix} v_1 \\ v_3 \\ \sigma_{33} \\ \sigma_{13} \end{pmatrix} = \mathbf{T}(z) \cdot \begin{pmatrix} U_P^- \\ U_S^- \\ U_P^+ \\ U_S^+ \end{pmatrix}, \tag{6.200}$$

where

$$\mathbf{T}(z) = \mathrm{i}\omega \begin{pmatrix} \beta_P & \beta_S & \beta_P & \beta_S \\ -\xi_P & -\xi_S & \xi_P & \xi_S \\ -Z_P & -Z_S & -Z_P & -Z_S \\ W_P & W_S & -W_P & -W_S \end{pmatrix}$$

$$\cdot \begin{pmatrix} \exp(\mathrm{i}\omega s_{3P} z) & 0 & 0 & 0 \\ 0 & \exp(\mathrm{i}\omega s_{3S} z) & 0 & 0 \\ 0 & 0 & \exp(-\mathrm{i}\omega s_{3P} z) & 0 \\ 0 & 0 & 0 & \exp(-\mathrm{i}\omega s_{3S} z) \end{pmatrix}, \tag{6.201}$$

with W and Z given in equations (6.121) and (6.123), respectively.

Then, the fields at $z = 0$ and $z = h$ are related by the following equation:

$$\mathbf{t}(0) = \mathbf{B} \cdot \mathbf{t}(h), \quad \mathbf{B} = \mathbf{T}(0) \cdot \mathbf{T}^{-1}(h), \tag{6.202}$$

which plays the role of a boundary condition. Note that when $h = 0$, $\mathbf{B}$ is the identity matrix.

Let us denote by the subscript 1 the upper half-space and by the subscript 2 the lower half-space. Moreover, the subscripts I, R and T denote the incident, reflected and transmitted waves. Using symmetry properties to define the polarization of the reflected waves, the particle velocities for a P wave incident from above the layer are given by

$$\mathbf{v}_1 = \mathbf{v}_{P_I} + \mathbf{v}_{P_R} + \mathbf{v}_{S_R}, \tag{6.203}$$

$$\mathbf{v}_2 = \mathbf{v}_{P_T} + \mathbf{v}_{S_T}, \tag{6.204}$$

where the particle velocities of the right-hand side have the same form as equations (6.133)-(6.137), where, here,

$$\begin{pmatrix} \beta_P \\ \xi_P \end{pmatrix} = \frac{1}{\sqrt{s_1^2 + s_{3P}^2}} \begin{pmatrix} s_1 \\ s_{3P} \end{pmatrix}, \qquad \begin{pmatrix} \beta_S \\ \xi_S \end{pmatrix} = \frac{1}{\sqrt{s_1^2 + s_{3S}^2}} \begin{pmatrix} s_{3S} \\ -s_1 \end{pmatrix}, \tag{6.205}$$

with

$$s_1^2 + s_{3P_i}^2 = \frac{\rho_i}{E_i} \equiv \frac{1}{v_{P_i}^2}, \quad s_1^2 + s_{3S_i}^2 = \frac{\rho_i}{\mu_i} \equiv \frac{1}{v_{S_i}^2}, \quad i = 1, 2, \tag{6.206}$$

where v_{P_i} and v_{S_i} are the complex compressional and shear velocities, respectively. On the other hand, the W and Z coefficients for the isotropic half-spaces are

$$W_{P_i} = 2\mu_i s_{3P_i} s_1 v_{P_i}, \qquad W_{S_i} = \mu_i (s_{3S_i}^2 - s_1^2) v_{S_i}, \tag{6.207}$$

$$Z_{P_i} = (\lambda_i s_1^2 + E_i s_{3P_i}^2) v_{P_i}, \quad Z_{S_i} = -2\mu_i s_{3S_i} s_1 v_{S_i}, \tag{6.208}$$

where $\lambda_i = E_i - 2\mu_i$ and μ_i are complex Lamé constants. Using equations (6.203) and (6.133)-(6.137), the particle-velocity/stress field at $z = 0$ can be expressed as

$$\mathbf{t}(0) = \mathbf{A}_1 \cdot \mathbf{r} + \mathbf{i}_P, \tag{6.209}$$

where

$$\mathbf{r} = (R_{\mathrm{PP}}, R_{\mathrm{PS}}, T_{\mathrm{PP}}, T_{\mathrm{PS}})^\top, \tag{6.210}$$

$$\mathbf{i}_P = \mathrm{i}\omega(\beta_{P_1}, \xi_{P_1}, -Z_{P_1}, -W_{P_1})^\top, \tag{6.211}$$

and

$$\mathbf{A}_1 = \mathrm{i}\omega \begin{pmatrix} \beta_{P_1} & \beta_{S_1} & 0 & 0 \\ -\xi_{P_1} & -\xi_{S_1} & 0 & 0 \\ -Z_{P_1} & -Z_{S_1} & 0 & 0 \\ W_{P_1} & W_{S_1} & 0 & 0 \end{pmatrix}. \tag{6.212}$$

Using equations (6.204) and (6.133)-(6.137), the particle-velocity/stress field at $z = h$ can be expressed as

$$\mathbf{t}(h) = \mathbf{A}_2 \cdot \mathbf{r}, \tag{6.213}$$

where

$$\mathbf{A}_2 = \mathrm{i}\omega \begin{pmatrix} 0 & 0 & \beta_{P_2}\exp(-\mathrm{i}\omega s_{3P_2}h) & \beta_{S_2}\exp(-\mathrm{i}\omega s_{3S_2}h) \\ 0 & 0 & \xi_{P_2}\exp(-\mathrm{i}\omega s_{3P_2}h) & \xi_{S_2}\exp(-\mathrm{i}\omega s_{3S_2}h) \\ 0 & 0 & -Z_{P_2}\exp(-\mathrm{i}\omega s_{3P_2}h) & -Z_{S_2}\exp(-\mathrm{i}\omega s_{3S_2}h) \\ 0 & 0 & -W_{P_2}\exp(-\mathrm{i}\omega s_{3P_2}h) & -W_{S_2}\exp(-\mathrm{i}\omega s_{3S_2}h) \end{pmatrix}. \tag{6.214}$$

Combining equations (6.202), (6.209) and (6.213) yields a matrix equation for the reflection- and transmission-coefficient array $\mathbf{r}$:

$$(\mathbf{A}_1 - \mathbf{B}\cdot\mathbf{A}_2)\cdot\mathbf{r} = -\mathbf{i}_P. \tag{6.215}$$

The reflection and transmission coefficients R_{SP}, R_{SS}, T_{SP} and T_{SS} for an incident S wave have the same scattering matrix as the P incident wave, but the array $\mathbf{i}_P$ is replaced by

$$\mathbf{i}_S = \mathrm{i}\omega(\beta_{S_1}, \xi_{S_1}, -Z_{S_1}, -W_{S_1})^\top. \tag{6.216}$$

In the absence of layer, $h = 0$, $\mathbf{B}$ is the identity matrix, and we get the system of equations obtained in Section 6.2.3. When the upper and lower half-spaces are the same medium, it can be shown that the absolute value of the PP-reflection coefficient at normal incidence is given by

$$R_{\mathrm{PP}}(0) = \frac{2|R_0\sin(kh)|}{|R_0^2\exp(-\mathrm{i}kh) - \exp(\mathrm{i}kh)|}, \tag{6.217}$$

where

$$k = \frac{\omega}{v_P}, \qquad v_P = \sqrt{\frac{p_{33}}{\rho}},$$

and

$$R_0 = \frac{\rho v_P - \rho_1 v_{P_1}}{\rho v_P + \rho_1 v_{P_1}},$$

with index 1 denoting the upper and the lower half-spaces. It is straightforward to generalize this approach for computing the seismic response of a stack of viscoelastic and anisotropic layers. We consider N layers with stiffnesses $p_{IJ\alpha}$, density ρ_α, each of them with thickness h_α, such that the total thickness is

$$h = \sum_{\alpha=1}^{N} h_\alpha. \tag{6.218}$$

By matching boundary conditions at the interfaces between layers, it is easy to show that the matrix system giving the reflection and transmission coefficients is

$$\left[\mathbf{A}_1 - \left(\prod_{\alpha=1}^{N}\mathbf{B}_\alpha\right)\cdot\mathbf{A}_2\right]\cdot\mathbf{r} = -\mathbf{i}_{P(S)}, \tag{6.219}$$

where $\mathbf{i}_{P(S)}$ is the incidence P(S) array, and

$$\mathbf{B}_\alpha = \mathbf{T}(0)\cdot\mathbf{T}^{-1}(h_\alpha), \quad \alpha = 1,\ldots,N. \tag{6.220}$$

This recursive approach, which is the basis of most reflectivity methods, dates back to Thomson (1950), and is illustrated by Brekhovskikh (1960, p. 61) for a stack of isotropic and elastic layers. An example of the application of this approach can be found in Carcione (2001b), where amplitude variations with offset (AVO) of pressure-seal reflections are investigated. Ursin and Stovas (2002) derive a second-order approximation for the reflection and transmission coefficients, which is useful for the inversion of seismic reflection data.